Glass transition in driven granular fluids: A mode-coupling approach

W. T. Kranz,[1,2] M. Sperl,[3] and A. Zippelius[1,2]

[1]*Georg-August-Universität Göttingen, Institut für Theoretische Physik, Friedrich-Hund-Platz 1, 37077 Göttingen, Germany*

[2]*Max-Planck-Institut für Dynamik und Selbstorganisation, Am Faßberg 17, 37077 Göttingen, Germany*

[3]*Institut für Materialphysik im Weltraum, Deutsches Zentrum für Luft- und Raumfahrt (DLR), 51170 Köln, Germany*

(Received 7 December 2012; revised manuscript received 5 February 2013; published 22 February 2013)

We consider the stationary state of a fluid comprised of inelastic hard spheres or disks under the influence of a random, momentum-conserving external force. Starting from the microscopic description of the dynamics, we derive a nonlinear equation of motion for the coherent scattering function in two and three space dimensions. A glass transition is observed for all coefficients of restitution, ε, at a critical packing fraction $\varphi_c(\varepsilon)$ below random close packing. The divergence of timescales at the glass transition implies a dependence on compression rate upon further increase of the density—similar to the cooling-rate dependence of a thermal glass. The critical dynamics for coherent motion as well as tagged particle dynamics is analyzed and shown to be nonuniversal with exponents depending on space dimension and degree of dissipation.

DOI: 10.1103/PhysRevE.87.022207 PACS number(s): 45.70.Cc, 64.70.qj, 47.57.Gc

I. INTRODUCTION

A wide range of fluids can be quenched into a disordered solid state. This includes metallic melts [1], colloidal suspensions [2], foams [3] and, recently, evidence was given that granular fluids may also undergo a glass transition [4–10]. Among all these different systems, colloidal suspensions are probably the best understood. Experiments by van Megen *et al.* [2,11] showed that, besides the fluid and the ordered crystalline phase, colloidal suspensions in thermal equilibrium can also form colloidal glasses: A dynamically arrested state of the system which is characterized by diverging relaxation times [12]. While a complete theoretical understanding of the glass transition in fragile glass formers is still missing [13], mode-coupling theories can quite successfully describe many of the phenomena on a quantitative level [14].

One interesting question has been raised more recently: Does the glass transition survive if the system is driven by external forcing into a nonequilibrium state? Or more generally, can one observe a glass transition also in a nonequilibrium system? A well-studied example is sheared colloidal suspensions for which it was shown that the equilibrium glass transition disappears [15,16]. Another example is nonlinear microrheology [17–19], where a strong pulling force is applied to a single particle, forcing it out of its cage, thereby possibly melting the glass.

Another system far from equilibrium is athermal packings of particles [20,21] undergoing a jamming transition at a critical packing fraction. Many of the properties close to the jamming point resemble those of fluids at the glass transition. This observation is at the heart of the jamming diagram, where the glass transition in thermal systems and the jamming transition are part of a larger parameter space [22,23].

Since granular particles are too large to be thermally activated, one necessarily needs a driving force to keep the grains in motion for extended periods of time. While in nature, gravity is probably the most important driving force [24], experimentalists have devised quite a few methods of fluidization. The list includes shaking [25], electrostatic [26,27] or magnetic [27,28] excitation, and fluidization by air [29,30] or water [31].

We have recently investigated the possibility of a glass transition in driven granular fluids. In two publications [9,10], henceforth referred to as I and II, we have demonstrated that mode-coupling theory (MCT) can be generalized to the far-from-equilibrium stationary state of a granular fluid. In particular, we found a granular glass transition for all degrees of dissipation, accompanied by the common signatures of a dense fluid close to the glass transition. Here, a careful derivation of the granular mode-coupling equations is presented and the consequences of MCT are worked out in detail. We furthermore extend our previous analysis to two-dimensional systems, which are realized in many experiments on granular matter [5,7,8,25,30]. The resulting glass transition diagram is shown in Fig. 1 in the plane spanned by packing fraction φ and coefficient of restitution, ε.

The dissipative interactions of the granular particles imply two primary consequences. First, while the dynamics of particles in thermal equilibrium is microscopically time-reversal invariant, the symmetry under time reversal is broken for granular dynamics. Second, there is no natural equilibrium reference state like for the sheared colloids [15,16], were the fluid can be thought of as being driven out of equilibrium by the optional external driving force. In the granular system, the driving force is required to maintain a stationary state with more than transient dynamics.

The paper is organized as follows: In Sec. II we define the model of a driven granular fluid and introduce the microscopic dynamics in Sec. III. In Sec. IV we derive the MCT equations for the coherent scattering function $\phi(q,t)$, discuss the asymptotic correlations $f_q := \phi(q,t \to \infty)$, which is used as an order parameter to locate the glass transition, and analyze the dynamics close to the glass transition. The MCT equations for the incoherent scattering function $\phi_s(q,t)$ of a tagged particle are derived in Sec. V. In Sec. VI we discuss our results in a broader context and conclude with a number of perspectives for future work in Sec. VII.

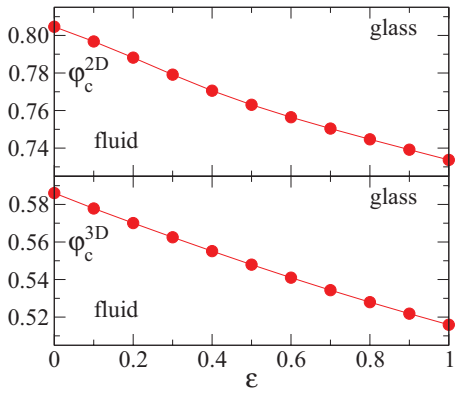

FIG. 1. (Color online) Critical packing fraction φ_c separating the fluid from the glassy state of driven granular particles as a function of the coefficient of restitution, ε, for space dimension $D = 2$ (top) and $D = 3$ (bottom).

II. MODEL

A. Inelastic hard spheres

The granular fluid is modeled as a monodisperse system of N smooth inelastic hard spheres (in dimension $D = 3$) or disks (in $D = 2$) of radius a and mass $m = 1$ in a volume $V = L^D$. We consider the thermodynamic limit $N, V \to \infty$ such that the density $n = N/V$ remains finite. Dissipation is introduced through a constant coefficient of normal restitution $\varepsilon \in [0,1]$ that augments the law of reflection [32],

$$\hat{\boldsymbol{r}}_{12} \cdot \boldsymbol{v}'_{12} = -\varepsilon\, \hat{\boldsymbol{r}}_{12} \cdot \boldsymbol{v}_{12}, \tag{1}$$

where $\boldsymbol{v}_{12} = \boldsymbol{v}_1 - \boldsymbol{v}_2$ is the relative velocity and $\hat{\boldsymbol{r}}_{12}$ is the unit vector pointing from the center of particle 2 to particle 1. The prime indicates postcollisional quantities.

B. Stochastic driving force

The driving force is implemented as an external random force,

$$\boldsymbol{v}'_i(t) = \boldsymbol{v}_i(t) + \sqrt{P_D}\, \boldsymbol{\xi}_i(t), \tag{2}$$

where P_D is the driving power. The ξ_i^α, $\alpha = 1, \ldots, D$ are Gaussian random variables with zero mean and variance,

$$\left\langle \xi_i^\alpha(t) \xi_j^\beta(t') \right\rangle_\xi = [\delta_{ij} - \delta_{\pi(i),j}]\delta^{\alpha\beta}\delta(t - t'), \tag{3}$$

where $\pi(i) = \arg\min_k\{|\boldsymbol{r}_i - \boldsymbol{r}_k| \geqslant \ell_D\}$ yields the index of the particle that is closest to particle i but at least a given distance ℓ_D away. In effect, the two particles i and $\pi(i)$ are driven by forces of equal strength but opposite direction. On length scales $\ell > \ell_D$, the driving force imparts no momentum on the system. Thereby, the external force does not destroy momentum conservation on length scales $\ell \gtrsim \ell_D$. We choose ℓ_D on the order of a mean particle separation.

C. The granular fluid

For undriven granular fluids, it is known that the homogeneous cooling state is unstable to shear fluctuations and eventually to density fluctuations [33,34]. In fact, the particles form extremely dense clusters. No such clustering instability is predicted [33], or indeed observed, for the randomly driven fluid. Consequently, we assume that the fluid is macroscopically homogeneous and isotropic. This implies that all spatial two-point correlation functions $C(\boldsymbol{r},\boldsymbol{r}')$ are functions of the distance $|\boldsymbol{r} - \boldsymbol{r}'|$ only.

Macroscopically, the fluid is fully characterized by the packing fraction φ (where $\varphi = \pi n d^3/6$ in $D = 3$ and $\varphi = \pi n d^2/4$ in $D = 2$), the coefficient of restitution, ε, and the driving power P_D. In the stationary state, the granular temperature $T = T(\varphi, \varepsilon, P_D) = \frac{1}{DN}\sum_i \boldsymbol{v}_i^2$ is given by the balance between the driving power P_D and the energy loss through the inelastic collisions.

The collision frequency $\omega_c \propto \sqrt{T}$ is the only time scale of the system. Thus, changing the granular temperature only changes the time scale of the system. To keep the discussion more transparent, we refrain from using the freedom to set $T = 1$ but keep in mind that the qualitative behavior of the system is independent of the temperature $T > 0$.

III. MICROSCOPIC DESCRIPTION

A. Observables

The two relevant observables discussed in the following are the density field $\rho(\boldsymbol{r},t)$ and the current density $\boldsymbol{j}(\boldsymbol{r},t)$ with the following microscopic definitions:

$$\rho(\boldsymbol{r},t) = \frac{1}{N}\sum_i \delta\left(\boldsymbol{r} - \boldsymbol{r}_i(t)\right), \tag{4a}$$

$$\boldsymbol{j}(\boldsymbol{r},t) = \frac{1}{N}\sum_i \boldsymbol{v}_i(t)\delta\left(\boldsymbol{r} - \boldsymbol{r}_i(t)\right). \tag{4b}$$

We will use the spatial Fourier transforms $\rho_{\boldsymbol{k}}(t) = \mathsf{FT}[\rho](\boldsymbol{k},t)$ [35] and the longitudinal current $j^L_{\boldsymbol{k}}(t) = \hat{\boldsymbol{k}} \cdot \mathsf{FT}[\boldsymbol{j}](\boldsymbol{k},t)$. The corresponding tagged particle quantities are given as

$$\rho^s(\boldsymbol{r},t) = \delta\left(\boldsymbol{r} - \boldsymbol{r}_s(t)\right), \tag{5a}$$

$$\boldsymbol{j}^s(\boldsymbol{r},t) = \boldsymbol{v}_s\delta\left(\boldsymbol{r} - \boldsymbol{r}_s(t)\right). \tag{5b}$$

B. Dynamics

The (forward in time) pseudo Liouville operator $\check{\mathcal{L}}_+$ describes the time evolution of a microscopic observable A, i.e., $i\check{\mathcal{L}}_+ A = dA/dt$, according to the dynamics specified above [36]. It is given as the sum of three parts,

$$\check{\mathcal{L}}_+(t) = \mathcal{L}_0 + \sum_{j<k}\mathcal{T}^+_{jk} + \check{\mathcal{L}}^+_D(t), \tag{6}$$

which are in turn (i) the free streaming operator $i\mathcal{L}_0 = \sum_j \boldsymbol{v}_j \cdot \boldsymbol{\nabla}_j$; (ii) the collision operator,

$$i\mathcal{T}^+_{jk} = -(\hat{\boldsymbol{r}}_{jk} \cdot \boldsymbol{v}_{jk})\,\Theta\left(-\hat{\boldsymbol{r}}_{jk} \cdot \boldsymbol{v}_{jk}\right)\delta(r_{jk} - d)(b^+_{jk} - 1), \tag{7}$$

where $\Theta(x)$ denotes the Heaviside step function and the operator b^+_{jk} implements the inelastic collision rule [37]; and (iii) the driving operator

$$i\check{\mathcal{L}}^+_D(t) = \sqrt{P_D}\sum_j \boldsymbol{\xi}_j(t) \cdot \left(\frac{\partial}{\partial \boldsymbol{v}_j} - \frac{\partial}{\partial \boldsymbol{v}_{\pi(j)}}\right). \tag{8}$$

With the binary collision expansion [38], formal power series of the pseudo Liouville operator can be defined. In

particular, this allows us to write the propagator $\check{\mathsf{U}}(t) = \exp_T \int_0^t \check{\mathcal{L}}_+(\tau)d\tau$ in terms of a time-ordered exponential [39]. The time ordering is needed because the driving part of the Liouville operator is explicitly time dependent.

C. Scattering functions

The central quantities in the following will be the coherent scattering function

$$\phi(q,t) = N\langle\langle\rho_{-\boldsymbol{q}}(0)\rho_{\boldsymbol{q}}(t)\rangle\rangle/S_q, \tag{9a}$$

where $S_q = N\langle\langle\rho_{-\boldsymbol{q}}\rho_{\boldsymbol{q}}\rangle\rangle$, and the incoherent scattering function

$$\phi_s(q,t) = \left\langle\left\langle\rho^s_{-\boldsymbol{q}}(0)\rho^s_{\boldsymbol{q}}(t)\right\rangle\right\rangle. \tag{9b}$$

Both correlation functions are introduced (cf. Appendix A) as expectation values $\langle\langle A(t)B(t')\rangle\rangle \equiv \langle\langle A(t)B(t')\rangle_\Xi\rangle := \int d\Gamma\varrho(\Gamma)\langle A(\Gamma,t)B(\Gamma,t')\rangle_\Xi$ with respect to the trajectory of the random driving force up to time t, $\Xi_t := \{(\boldsymbol{\xi}_1(\tau),\ldots,\boldsymbol{\xi}_N(\tau))|0 \leqslant \tau \leqslant t\}$ and to the stationary phase space distribution function $\varrho(\Gamma)$. Here, $\Gamma := (\boldsymbol{r}_1,\boldsymbol{v}_1,\ldots,\boldsymbol{r}_N,\boldsymbol{v}_N)$ denotes a location in phase space.

In contrast to fluids in equilibrium, no analytical expression for the stationary phase space distribution of driven granular fluids is known so far. Therefore we have to make a few assumptions to evaluate the expectation values. First of all we assume that positions and velocities are uncorrelated; $\varrho(\Gamma) = \varrho_r(\{\boldsymbol{r}_i\})\varrho_v(\{\boldsymbol{v}_i\})$. Moreover, we assume that the velocity distribution factorizes into a product of one particle distribution functions, $\varrho_v(\{\boldsymbol{v}_i\}) = \prod_i \varrho_1(\boldsymbol{v}_i)$. All we need to know about $\varrho_1(\boldsymbol{v})$ is that it has a vanishing first moment, $\int d^D v\, \boldsymbol{v}\varrho_1(\boldsymbol{v}) = 0$ and a finite second moment, $\int d^D v\, v^2\varrho_1(\boldsymbol{v}) = DT < \infty$. The spatial distribution function $\varrho_r(\{\boldsymbol{r}_i\})$ enters the theory via the static correlation function, as will be discussed below.

In general, all macroscopic quantities will be functions of the coefficient of restitution ε. To reduce clutter, we will suppress this dependence.

D. Static structure factors

Below, we will treat the static structure functions as a known input. Hence, we need $S_q = S_q(\varphi,\varepsilon)$ for a range of densities φ around where we expect the critical density to be. Lacking good quality data for $S_q(\varphi \sim \varphi_c(\varepsilon),\varepsilon)$, let alone reliable theoretical predictions for this quantity, we use preliminary results that $S_q(\varphi,\varepsilon)$ only weakly depends on the coefficient of restitution ε and approximate $S_q(\varphi,\varepsilon) \approx S_q(\varphi,\varepsilon = 1)$ by their elastic counterparts: In $D = 3$ we use the Percus-Yevick (PY) equation [40] for elastic hard spheres in thermal equilibrium [41], except for the pair correlation function at contact which is better approximated by the Carnahan-Starling expression [42]. In $D = 2$ we use the Baus-Colot (BC) equation [43] throughout.

E. Effective dynamics

Because the density $\rho_{\boldsymbol{q}}$ does not depend on the driving force Ξ_t explicitly, the coherent scattering function

$$\phi(q,t) = \langle\langle\rho_{-\boldsymbol{q}}\check{\mathsf{U}}(t)\rho_{\boldsymbol{q}}\rangle_\Xi\rangle = \langle\rho_{-\boldsymbol{q}}\mathsf{U}(t)\rho_{\boldsymbol{q}}\rangle \tag{10}$$

can be given in terms of an average propagator $\mathsf{U}(t) = \langle\check{\mathsf{U}}(t)\rangle_\Xi$. The same argument holds for the incoherent scattering function $\phi_s(q,t)$. Associated with this average propagator is an effective, time-independent pseudo Liouville operator, $\mathsf{U}(t) = \exp(it\mathcal{L}_+) := \sum_n (it\mathcal{L}_+)^n/n!$. There is no need for time ordering anymore.

A standard procedure [39] shows that the effective pseudo Liouville operator is given as

$$\mathcal{L}_+ = \mathcal{L}_0 + \sum_{j<k}\mathcal{T}^+_{jk} + \mathcal{L}^+_D, \tag{11}$$

where $\mathcal{L}^+_D = P_D\sum_j \frac{\partial^2}{\partial \boldsymbol{v}_j}$. From here on, we will only use the effective dynamics.

Averages over pairs of observables define a scalar product, $\langle A|B\rangle := \langle A^*B\rangle$ where A^* denotes the complex conjugate of A. Given the definition of a scalar product, we can formally introduce the adjoint Liouville operator $\mathcal{L}^\dagger_+$ via the relation $\langle\mathcal{L}^\dagger_+A|B\rangle = \langle A|\mathcal{L}_+B\rangle$. For elastic hard spheres in thermal equilibrium, it can be shown that detailed balance implies $\mathcal{L}^\dagger_+(\varepsilon = 1) = \mathcal{L}_-(\varepsilon = 1)$, where $\mathcal{L}_-$ is the Liouville operator describing time-reversed dynamics. This relation does not hold for inelastic collisions which are discussed here. In the present context, an explicit expression for $\mathcal{L}^\dagger_+$ is not needed and hence will be given elsewhere.

The homogeneity of the system is reflected in the matrix elements

$$\langle A_1(\boldsymbol{k}_1)\cdots A_n(\boldsymbol{k}_n)|B_1(\boldsymbol{p}_1)\cdots B_m(\boldsymbol{p}_m)\rangle \propto \delta_{\sum \boldsymbol{k}_i,\sum \boldsymbol{p}_i}$$

in the form of a selection rule. Here, the $A_i(\boldsymbol{k}_i)$, $B_i(\boldsymbol{p}_i)$ are arbitrary microscopic observables and $\boldsymbol{k}_i$, $\boldsymbol{p}_i$ are wave vectors.

The starting point for the derivation of equations of motion is an operator identity that is most concisely expressed in the Laplace domain [44],

$$\mathcal{P}\hat{\mathsf{U}}(s)\mathcal{P} = [s - \Omega - \hat{\mathsf{M}}(s)]^{-1}, \tag{12}$$

where $\Omega = \mathcal{P}\mathcal{L}_+\mathcal{P}$,

$$\mathsf{M}(t) = \mathcal{P}\mathcal{L}_+\mathcal{Q}\exp(it\mathcal{Q}\mathcal{L}_+\mathcal{Q})\mathcal{Q}\mathcal{L}_+\mathcal{P}, \tag{13}$$

and $\mathcal{P} = \mathcal{P}^2$, $\mathcal{Q} = 1 - \mathcal{P}$ are projection operators [45]. The Laplace-transformed propagator $\hat{\mathsf{U}}(s) \equiv \mathsf{LT}[\mathsf{U}](s) = (s - \mathcal{L}_+)^{-1}$ is defined as a power series.

IV. GRANULAR GLASS TRANSITION

A. Equations of motion

Let us introduce the following microscopic state vector: $\boldsymbol{a}_{\boldsymbol{q}} = \sqrt{N}(\rho_{\boldsymbol{q}}/\sqrt{S_q}, j^L_{\boldsymbol{q}}/\sqrt{T})$. Then the coherent scattering function $\phi(q,t)$ is given as one element of the matrix of correlators $\Phi(q,t) = \langle\boldsymbol{a}_{\boldsymbol{q}}|\mathsf{U}(t)\boldsymbol{a}_{\boldsymbol{q}}\rangle$.

With the help of Eq. (12) and the coherent projectors

$$\mathcal{P}_c = N\sum_{\boldsymbol{q}}|\rho_{\boldsymbol{q}}\rangle\langle\rho_{\boldsymbol{q}}|/S_q + \sum_{\boldsymbol{q}}\left|j^L_{\boldsymbol{q}}\right\rangle\left\langle j^L_{\boldsymbol{q}}\right|/\left\langle j^L_{\boldsymbol{q}}|j^L_{\boldsymbol{q}}\right\rangle, \tag{14}$$

$\mathcal{Q}_c = 1 - \mathcal{P}_c$, one finds

$$\hat{\Phi}^{-1}(q,s) = \begin{pmatrix} s & -\Omega_{\rho j}(q)[1 + \hat{L}(q,s)] \\ -\Omega_{j\rho}(q) & s - i\nu_q - \hat{M}(q,s) \end{pmatrix}, \tag{15}$$

while $\Omega_{\rho\rho} \propto \langle \rho_{\boldsymbol{q}} | \mathcal{L}_+ \rho_{\boldsymbol{q}} \rangle = q \langle \rho_{\boldsymbol{q}} | j^L_{\boldsymbol{q}} \rangle = 0$ due to the assumed symmetry of the velocity distribution. The other entries of the frequency matrix $\Omega_{ab} = \langle \boldsymbol{a}_{\boldsymbol{q}} | \Omega \boldsymbol{a}_{\boldsymbol{q}} \rangle$ are nonzero [note that $i\nu_q = \Omega_{jj}(q)$].

The memory kernels are formally given as

$$M(q,t) = N \langle F^\dagger_{\boldsymbol{q}} | \tilde{\mathsf{U}}(t) F_{\boldsymbol{q}} \rangle / T, \tag{16a}$$

$$L(q,t) = \langle J^\dagger_{\boldsymbol{q}} | \tilde{\mathsf{U}}(t) F_{\boldsymbol{q}} \rangle \big/ \langle \rho_{\boldsymbol{q}} | \mathcal{L}_+ j^L_{\boldsymbol{q}} \rangle, \tag{16b}$$

where $\tilde{\mathsf{U}}(t) = \exp(it\mathcal{Q}_c\mathcal{L}_+\mathcal{Q}_c)$ is a modified propagator. There are two fluctuating forces, $F_{\boldsymbol{q}} = \mathcal{Q}_c\mathcal{L}_+ j^L_{\boldsymbol{q}}$ and $F^\dagger_{\boldsymbol{q}} = \mathcal{Q}_c\mathcal{L}^\dagger_+ j^L_{\boldsymbol{q}}$, and at this point we cannot rule out that there is a nonzero fluctuating current, $J^\dagger_{\boldsymbol{q}} = \mathcal{Q}_c\mathcal{L}^\dagger_+\rho_{\boldsymbol{q}}$, while $J_{\boldsymbol{q}} = \mathcal{Q}_c\mathcal{L}_+\rho_{\boldsymbol{q}} = q\mathcal{Q}_c j^L_{\boldsymbol{q}} = 0$. In the elastic limit $F^\dagger_{\boldsymbol{q}} = F_{\boldsymbol{q}}$ and $J^\dagger_{\boldsymbol{q}} = J_{\boldsymbol{q}} = 0$ holds and therefore $L(q,t)$ vanishes.

In the Laplace domain, the coherent scattering function is thus given as

$$\hat{\phi}^{-1}(q,s) = s - \frac{\Omega_q^2[1 + \hat{L}(q,s)]}{s - i\nu_q - \hat{M}(q,s)}, \tag{17}$$

where $\Omega_q^2 = \Omega_{\rho j}\Omega_{j\rho}$ or, equivalently, in the time domain as the solution of the equation of motion,

$$\begin{aligned} 0 = {} & \ddot{\phi}(q,t) + \nu_q\dot{\phi}(q,t) + \Omega_q^2\phi(q,t) \\ & + \Omega_q^2 \int_0^t d\tau\, m(q,t-\tau)\dot{\phi}(q,\tau) \\ & + \Omega_q^2 \int_0^t d\tau\, L(q,t-\tau)\phi(q,\tau), \end{aligned} \tag{18}$$

where $m(q,t) = M(q,t)/\Omega_q^2$ and the initial conditions are $\dot{\phi}(q,t=0) = 0$ and $\phi(q,t=0) = 1$.

Note that, while the memory kernel $M(q,t)$ is defined as a dynamic correlation function in Eq. (16a), it is a cross-correlation function in general and an autocorrelation function only in the elastic limit $\varepsilon = 1$. For $\varepsilon < 1$, the memory kernel $M(q,t)$ is still a fluctuating force correlator, modified by the inelasticity of the interactions. While the memory kernel $L(q,t)$ vanishes exactly in the elastic limit, in inelastic systems it quantifies through a fluctuating current $J^\dagger_{\boldsymbol{q}}$ the violation of detailed balance. Within the mode-coupling approximation discussed below, the memory kernel $L(q,t)$ vanishes and plays no further role.

To proceed, we need to find approximate expressions for the memory kernels. Before we come to the mode-coupling approximation, we discuss the simpler assumption that $M(q,t) = L(q,t) = 0$.

B. Sound waves

The linear equation of motion

$$\ddot{\phi}(q,t) + \nu_q\dot{\phi}(q,t) + \Omega_q^2\phi(q,t) = 0 \tag{19}$$

describes damped sound waves $\phi(q,t) = e^{-\nu_q t/2}\cos(C_q q t)$.

Sound damping due to collisions, as described by the second term in Eq. (19),

$$i\nu_q = N \big\langle j^L_{\boldsymbol{q}} \big| \mathcal{L}_+ j^L_{\boldsymbol{q}} \big\rangle \big/ T, \tag{20}$$

can be evaluated with Enskog's method [46,47]. The calculation for two dimensions is shown in Appendix C 1, yielding

$$\nu_q = \frac{1+\varepsilon}{2}\omega_E[1 + 2J_0''(qd)] \tag{21a}$$

in $D = 2$, where $J_0(x)$ is the zeroth-order Bessel function [48] and the double prime denotes the second derivative with respect to the argument. The result in three dimensions is known [47]:

$$\nu_q = \frac{1+\varepsilon}{3}\omega_E[1 + 3j_0''(qd)] \tag{21b}$$

in $D = 3$, where $j_0(x) = \sin(x)/x$ is the zeroth-order spherical Bessel function [49]. The Enskog collision frequency $\omega_E = 2^D D(\varphi\chi/d)\sqrt{T/\pi}$ is given in terms of the contact value, χ, of the pair correlation function [50].

The wave-number dependent speed of sound is given by $C_q^2 = \Omega_q^2/q^2 = \Omega_{\rho j}\Omega_{j\rho}/q^2$. One finds

$$\begin{aligned} \Omega_{j\rho} &= N \big\langle j^L_{\boldsymbol{q}} \big| \mathcal{L}_+ \rho_{\boldsymbol{q}} \big\rangle \big/ \sqrt{T S_q} \\ &= q S_{\ell\ell}(q) \sqrt{T/S_q}, \end{aligned} \tag{22a}$$

with the longitudinal current correlator $S_{\ell\ell}(q) := N\langle j^L_{\boldsymbol{q}} | j^L_{\boldsymbol{q}} \rangle / T$. The calculation (cf. Appendix C 2) of

$$\Omega_{\rho j} = \frac{N}{\sqrt{T S_q}} \big\langle \rho_{\boldsymbol{q}} \big| \mathcal{L}_+ j^L_{\boldsymbol{q}} \big\rangle \tag{22b}$$

$$\approx q\sqrt{T/S_q}\left(\frac{1+\varepsilon}{2} + \frac{1-\varepsilon}{2}S_q\right) \tag{22b}$$

uses the approximate granular Yvon-Born-Green (YBG) relation (cf. Appendix B). Combining these results, we find that the speed of sound

$$C_q^2 = T\frac{S_{\ell\ell}(q)}{S_q}\left(\frac{1+\varepsilon}{2} + \frac{1-\varepsilon}{2}S_q\right) \tag{23}$$

is reduced for the dissipative driven fluid compared to a fluid of elastic hard spheres in thermal equilibrium. The sound damping $\nu_q/(2q^2)$, on the other hand, decreases with increasing dissipation.

Alternatively, the speed of sound can be given as $C_q^2 = S_{\ell\ell}(q)/(n\kappa_q^{\text{eff}})$, where the effective compressibility κ_q^{eff} is defined in a form

$$\frac{1}{\kappa_q^{\text{eff}}} = \frac{1}{\kappa_q^0} + \frac{1-\varepsilon}{2}Tn^2c_q, \tag{24}$$

reminiscent of a random phase approximation [51]. Here, $\kappa_q^0 = S_q/(nT)$ is the compressibility of a fictitious elastic hard sphere system with a structure factor S_q and c_q is the direct correlation function [50].

We close this section with a few remarks. First, in a thermal fluid the expression for the sound velocity simplifies, because $S_{\ell\ell}(q) \equiv 1$ due to molecular chaos [52]. In a granular fluid, $S_{\ell\ell}(q)$ is actually found to be wave-number dependent. Preliminary results indicate $S_{\ell\ell}(q \to 0) < 1$. Second, from $\Omega_{\rho j} \neq \Omega_{j\rho}$ for $\varepsilon < 1$, it can be seen explicitly that the Liouville operator is not self-adjoint. In terms of physical processes, this reflects the transition rate for the conversion of density fluctuations into current fluctuations not being equal to the rate of the reverse process. Detailed balance or more general time-reversal invariance is broken already for the

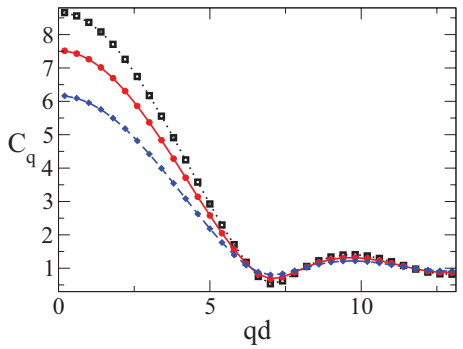

FIG. 2. (Color online) Speed of sound C_q according to Eq. (23) as a function of wave number q in 3D for packing fraction $\varphi = 0.516$ and coefficient of restitution $\varepsilon = 1.0$ (squares), 0.5 (filled circles), and 0.0 (diamonds).

linear equation of motion (cf. Sec. V A below). Finally, it is known [50] that Navier-Stokes–order hydrodynamics does not exist in $D = 2$, presumably implying logarithmic corrections to the sound damping in $D = 2$.

In the following, we set $S_{\ell\ell}(q) \equiv 1$. In Fig. 2, the resulting sound dispersion relations are shown for the packing fraction $\varphi = 0.516$ and the coefficient of restitution varying from $\varepsilon = 1$ to 0. The speed of sound decreases with increasing dissipation, in agreement with hydrodynamic predictions [53].

C. Mode-coupling approximation

In the spirit of the equilibrium mode-coupling theories [54–57], we introduce a second projection operator

$$\mathcal{P}_2 = \sum_{\boldsymbol{k}<\boldsymbol{p}} |\rho_{\boldsymbol{k}}\rho_{\boldsymbol{p}}\rangle\langle\rho_{\boldsymbol{k}}\rho_{\boldsymbol{p}}|/\langle\rho_{\boldsymbol{k}}\rho_{\boldsymbol{p}}|\rho_{\boldsymbol{k}}\rho_{\boldsymbol{p}}\rangle \tag{25}$$

and approximate the modified propagator as

$$\begin{aligned}\tilde{\mathsf{U}}(t) &\approx \mathcal{P}_2\tilde{\mathsf{U}}(t)\mathcal{P}_2 \\ &\approx N^2 \sum_{\boldsymbol{k}<\boldsymbol{p}} |\rho_{\boldsymbol{k}}\rho_{\boldsymbol{p}}\rangle\phi(k,t)\phi(p,t)\langle\rho_{\boldsymbol{k}}\rho_{\boldsymbol{p}}|/(S_kS_p),\end{aligned} \tag{26}$$

where a factorization approximation,

$$\langle\rho_{\boldsymbol{k}}\rho_{\boldsymbol{p}}|\tilde{\mathsf{U}}(t)\rho_{\boldsymbol{k}}\rho_{\boldsymbol{p}}\rangle\langle\rho_{\boldsymbol{k}}\rho_{\boldsymbol{p}}|\rho_{\boldsymbol{k}}\rho_{\boldsymbol{p}}\rangle \approx \phi(k,t)\phi(p,t),$$

was employed. Equation (26) is known as the mode-coupling approximation (MCA).

1. Mode-coupling approximation of L

We find

$$L(q,t) \approx \frac{N}{qT}\sum_{\boldsymbol{k}<\boldsymbol{p}} \mathcal{U}_{\boldsymbol{qkp}}\mathcal{W}_{\boldsymbol{qkp}}\phi(k,t)\phi(p,t), \tag{27}$$

where

$$\mathcal{U}_{\boldsymbol{qkp}} = N\langle\rho_q|\mathcal{L}_+\mathcal{Q}_c\rho_{\boldsymbol{k}}\rho_{\boldsymbol{p}}\rangle/S_k = 0 \tag{28}$$

due to parity and where $\mathcal{W}_{\boldsymbol{qkp}}$ is defined below. Therefore $L(q,t) \equiv 0$ within the mode-coupling approximation.

2. Mode-coupling approximation of M

The mode-coupling approximation for $M(q,t)$ yields

$$M(q,t) \approx \frac{N}{T}\sum_{\boldsymbol{k}<\boldsymbol{p}} \mathcal{V}_{\boldsymbol{qkp}}\mathcal{W}_{\boldsymbol{qkp}}\phi(k,t)\phi(p,t), \tag{29}$$

where

$$\mathcal{V}_{\boldsymbol{qkp}} = N\langle j_{\boldsymbol{q}}^L|\mathcal{L}_+\mathcal{Q}_c\rho_{\boldsymbol{k}}\rho_{\boldsymbol{p}}\rangle/S_k, \tag{30a}$$

$$\mathcal{W}_{\boldsymbol{qkp}} = N\langle\rho_{\boldsymbol{k}}\rho_{\boldsymbol{p}}|\mathcal{Q}_c\mathcal{L}_+ j_q^L\rangle/S_p. \tag{30b}$$

The left vertex is known from the literature [58]:

$$\begin{aligned}\mathcal{V}_{\boldsymbol{qkp}} = \frac{T}{NS_k}&[(\hat{\boldsymbol{q}}\cdot\boldsymbol{k})S_p + (\hat{\boldsymbol{q}}\cdot\boldsymbol{p})S_k \\ &- qS^{(3)}(\boldsymbol{k},\boldsymbol{p})/S_q]\delta_{\boldsymbol{q},\boldsymbol{k}+\boldsymbol{p}}.\end{aligned}$$

Customarily, the convolution approximation [59] $S^{(3)}(\boldsymbol{k},\boldsymbol{p}) \approx S_kS_pS_q$ is applied to yield

$$\mathcal{V}_{\boldsymbol{qkp}} = \frac{T}{N}S_p[(\hat{\boldsymbol{q}}\cdot\boldsymbol{k})nc_k + (\hat{\boldsymbol{q}}\cdot\boldsymbol{p})nc_p]\delta_{\boldsymbol{q},\boldsymbol{k}+\boldsymbol{p}}. \tag{31a}$$

By a nontrivial calculation (see Appendix C 3), we were able to show that the right vertex is approximately given as

$$\mathcal{W}_{\boldsymbol{qkp}} \approx \frac{1+\varepsilon}{2}\frac{T}{N}S_k[(\hat{\boldsymbol{q}}\cdot\boldsymbol{k})nc_k + (\hat{\boldsymbol{q}}\cdot\boldsymbol{p})nc_p]\delta_{\boldsymbol{q},\boldsymbol{k}+\boldsymbol{p}}, \tag{31b}$$

which is different from $\mathcal{V}_{\boldsymbol{qkp}}$.

The physical interpretation of these results for the vertices is that (i) the rate of annihilation of pairs of density fluctuations $\rho_{\boldsymbol{k}}$, $\rho_{\boldsymbol{p}}$ is determined by the static structure of the fluid, both in an equilibrium fluid and in the driven granular fluid; (ii) the rate of creation of such density fluctuations is suppressed by a factor $(1+\varepsilon)/2$, though, compared with the rate of creation or with the equivalent rate in an equilibrium fluid.

The reduced memory kernel in the mode-coupling approximation (reported in I) then reads

$$\begin{aligned}&m[\phi](q,t) \\ &= A_q(\varepsilon)\frac{nS_q}{q^2}\int\frac{d^Dk}{(2\pi)^D}S_kS_{|\boldsymbol{q}-\boldsymbol{k}|} \\ &\quad\times\{[\hat{\boldsymbol{q}}\cdot\boldsymbol{k}]c_k + [\hat{\boldsymbol{q}}\cdot(\boldsymbol{q}-\boldsymbol{k})]c_p\}^2\phi(k,t)\phi(|\boldsymbol{q}-\boldsymbol{k}|,t),\end{aligned} \tag{32}$$

where

$$A_q^{-1}(\varepsilon) = 1 + \frac{1-\varepsilon}{1+\varepsilon}S_q. \tag{33}$$

Figure 3 demonstrates the prefactor $A_q(\varepsilon)$ that distinguishes the granular memory functions from the well-known elastic results where $A_q(\varepsilon = 1.0) = 1$: For $\varepsilon < 1$, the prefactor exhibits deviations from unity with oscillations given by the static structure factor. As $A_q(\varepsilon)$ is minimal for the first peak of the structure factor, i.e., the length scale of the cage, one concludes that increasing dissipation (decreasing coefficient of restitution) weakens the cage effect. Compared to the elastic case, the force acting by the cage onto the particles inside the cage is smaller as the particles' reflections from each other are reduced by the influence of dissipation. While additional changes are expected by the ε dependence of the structure factors, the major difference is encoded in the prefactor $A_q(\varepsilon)$. The fact that $A_q(\varepsilon) > 0$ for all values of the coefficient of restitution ε ensures that the memory kernel remains positive.

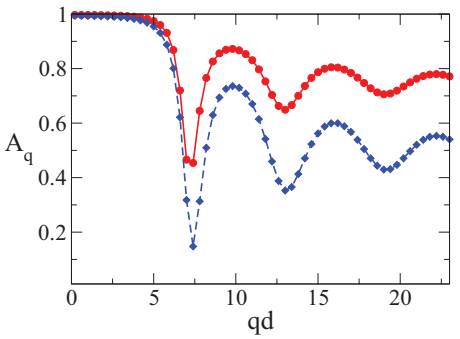

FIG. 3. (Color online) Prefactor of memory kernel $A_q(\varepsilon)$ as a function of wave number q for two values of the coefficient of restitution, $\varepsilon = 0.5$ (filled circles) and 0.0 (diamonds), in 3D.

D. Approximate equation of motion and phase diagram

With the mode-coupling approximations in place, the equation of motion

$$0 = \ddot{\phi}(q,t) + \nu_q \dot{\phi}(q,t) + \Omega_q^2 \phi(q,t) + \Omega_q^2 \int_0^t d\tau\, m[\phi](q,t-\tau)\dot{\phi}(q,\tau) \qquad (34)$$

turns into a closed equation for the coherent scattering function once the static structure factor S_q is known. This equation of motion has the same formal structure as the one for the elastic hard-sphere fluid in thermal equilibrium. The viscous term, Eq. (20), decreases with decreasing coefficient of restitution ε; the speed of sound, Eq. (23), acquires a nontrivial dependence on the coefficient of restitution as does the memory kernel $m[\phi]$.

Structural arrest of the grains in a glassy state gives rise to time-persistent density correlations. Hence, we introduce the order parameter for the glass transition, $f_q := \lim_{t\to\infty} \phi(q,t)$. It can readily be shown that the above equation of motion yields the following equation for the asymptotic function f_q:

$$\frac{f_q}{1-f_q} = m[f](q). \qquad (35)$$

With the memory kernel being independent of temperature, the order parameter f_q is also independent of temperature, as expected. It can easily be checked that $f_q \equiv 0$ is always a solution of the above equation. Studying this equation from a dynamical-systems point of view, one finds that, at a critical density φ_c, the vanishing solution becomes unstable and a new, stable solution $f_q > 0$ appears discontinuously, signaling the glass transition [14]. The order parameter at the critical density φ_c will be denoted as f_q^c.

Using the structure factors as discussed in Sec. III D, we find the phase diagrams in Fig. 1 for $D = 3$ (as reported in I) and $D = 2$ (for technical parameters cf. Appendix D). The order parameter jumps discontinuously at the critical density φ_c as expected [14] from the type of singularity in Eq. (35). The evolution of the transition with ε is remarkably similar for two dimensions (2D) and three dimensions (3D), with transition densities increasing from the elastic case to $\varepsilon = 0.0$ by around 10% in a roughly linear fashion.

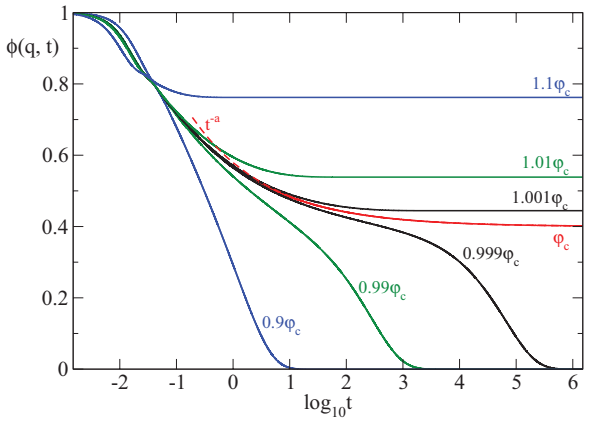

FIG. 4. (Color online) Coherent scattering functions $\phi(q,t)$ as a function of time t in 3D for wave number $qd = 4.2$. At the transition point at packing fraction $\varphi^c(\varepsilon = 0.5) = 0.548$ with a critical glass-form factor of $f_q^c = 0.400$, and at higher ($1.1\varphi^c$, $1.01\varphi^c$, $1.001\varphi^c$) and lower ($0.9\varphi^c$, $0.99\varphi^c$, $0.999\varphi^c$) packing fractions. The exponent parameter is $\lambda = 0.710$ which yields the critical exponent $a = 0.323$ and von Schweidler exponent $b = 0.624$. The critical amplitude for $qd = 4.2$ is $h_q = 0.583$. The critical law labeled t^{-a} is shown as a dashed curve for a time scale $t_0 = 0.0260$.

E. Coherent dynamics close to glass transition

The full dynamics of density fluctuations is obtained by solving the MCT equations by iteration (for details, see Appendix D). In Figs. 4 and 5 we show the coherent scattering function in $D = 3$ for several densities, below and above the critical point for $\varepsilon = 0.5$ and two wave numbers $qd = 4.2$ and $qd = 7$. As the critical point is approached from the fluid side, one observes the development of a plateau in the coherent scattering function. Increasing the density above the critical value φ_c leads to an increase in the order parameter f_q [60].

The MCT equations of motion are known to admit scaling solutions close to the critical point [14,61]. As the granular mode-coupling equations are formally identical to those for

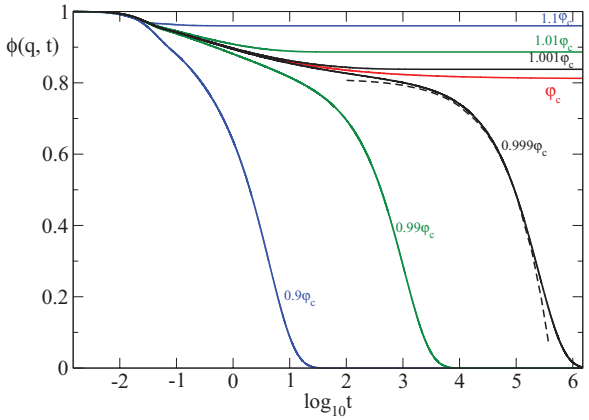

FIG. 5. (Color online) Coherent scattering functions $\phi(q,t)$ as a function of time t in 3D (cf. Fig. 4) for a different wave number $qd = 7$. The critical amplitude for $qd = 7$ is $h_q = 0.367$. The von Schweidler law is shown as a dashed curve for a fitting time scale $\tau = 1.21 \times 10^5$.

an equilibrium hard-sphere fluid, the scaling analysis is also closely related. To keep the presentation self-contained, we will summarize the main results of this analysis. The analogous analysis for the incoherent scattering function discussed below in Sec. V was presented in II.

At small distances $\sigma(\varepsilon) := [\varphi_c(\varepsilon) - \varphi]/\varphi_c(\varepsilon)$ to the critical point, one finds

$$\phi(q,t;\,\sigma) = f_q^c + h_q G_\sigma(t), \tag{36}$$

where $h_q = h_q(\varepsilon)$ is the critical amplitude and $G_\sigma(t)$ is a scaling function, independent of the wave number. The scaling function $G_\sigma(t)$ can be characterized by a hierarchy of time scales. The shortest time scale is naturally provided by the mean time between collisions, $t_0 \equiv \omega_c^{-1}$. The time scale t_σ for the transition through the plateau, where $\phi(q,t_\sigma;\;\sigma) = f_q^c$, diverges at the glass transition as $t_\sigma \propto \sigma^{-\delta}$ where $\delta = 1/(2a)$. For short but macroscopic times, in the β regime, one finds

$$G_\sigma(t) \propto (t/t_0)^{-a}, \quad t_0 \ll t \leqslant t_\sigma. \tag{37a}$$

For larger times, $t \geqslant t_\sigma$ but still well below the so-called α-relaxation time scale τ,

$$G_\sigma(t) \propto -(t/t_\sigma)^b, \quad t_\sigma \leqslant t \ll \tau. \tag{37b}$$

Finally, for the largest times the time-density superposition principle holds, i.e., the coherent scattering functions can be collapsed onto a master curve

$$\phi(q,t;\,\sigma) = \tilde{\phi}\,(q,t/\tau(q;\,\sigma))\,. \tag{38}$$

The time scale τ diverges at the glass transition, $\tau = \tau(q;\;\sigma) \propto \sigma^{-\gamma}$ where $\gamma = 1/(2a) + 1/(2b)$. An empirical choice for the scaling function $\tilde{\phi}(q,t)$ is provided by the Kohlrausch-Williams-Watts law $\tilde{\phi}_{\mathrm{KWW}}(q,t) \propto \exp(-t^\beta)$ [62], crossing over to an exponential decay for the longest times [63]. The power laws discussed above are valid in the asymptotic regime close to the transition. The validity may hence be preempted by the potential importance of decay processes not captured by MCT [13].

The critical exponents a, b in Eqs. (37) are related to a single-exponent parameter $\lambda = \lambda(D,\varepsilon)$ by the universal relation

$$\lambda = \frac{\Gamma^2(1-a)}{\Gamma(1-2a)} = \frac{\Gamma^2(1+b)}{\Gamma(1+2b)}, \tag{39}$$

where $\Gamma(x)$ is the Euler Gamma function.

The sets of exponents shown in Figs. 6 and 7 in 3D and 2D, respectively, are functions of the dimension but differ only slightly between $D = 2$ and $D = 3$. Overall, there is a tendency for the exponents in Figs. 6 and 7 to show slightly lesser stretching for higher dissipation, i.e., smaller ε. This may be interpreted as the more dissipative and also more strongly driven fluid experiencing less distinctive features in its glassy dynamics. The divergence in time scales is also expected to be a bit less pronounced. While the predicted changes in exponents are most likely hard to detect in experiment and simulation as absolute numbers, one should be able to detect the changes in comparison of different degrees of dissipation. Especially, the master functions should be comparably sensitive to changes in the exponents a and b.

It is seen in Fig. 8 that for smaller ε the order parameter f_q^c decays more slowly for large wave numbers, indicating a tighter localization. In comparison to 3D, the transition in 2D exhibits individually sharper peaks and overall a tighter localization for the same dissipation; cf. Fig. 9. It has been shown for data from simulation [64] and experiments in colloidal suspensions [2,65], that the MCT predictions for the f_q^c are typically accurate to around 20%. Hence, rather than fitting individual f_q^c directly to measurements and numerical calculations, experimental and simulation data can be expected to follow the distributions shown on the 20% level and exhibit trends with variation of ε as indicated here.

It is seen in Fig. 4 that the critical law can only be observed without corrections for states closer than 0.1% to the transition point. Also, the von Schweidler law in Fig. 5 is only valid for an intermediate regime after the plateau. The regimes of applicability for the asymptotic scaling laws are therefore similar to the elastic case, and corrections to scaling are expected to follow the known trends [60].

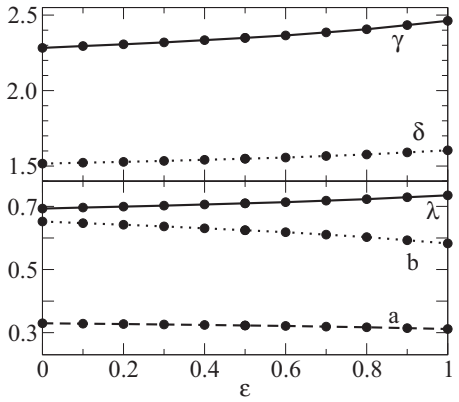

FIG. 6. Complete set of exponents in 3D as a function of the coefficient of restitution ε. The top panel shows the exponents δ and γ for the divergence of the time scales. The lower panel shows the exponents a and b for the master functions and the exponent parameter λ.

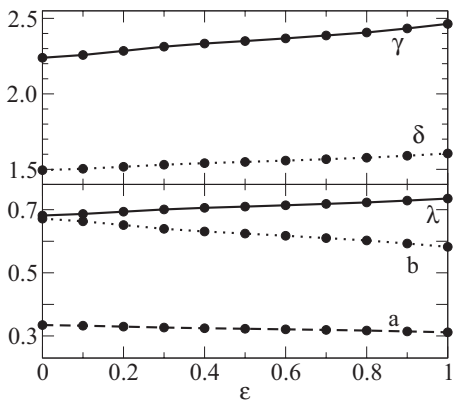

FIG. 7. Complete set of exponents in 2D as function of the coefficient of restitution ε. The top panel shows the exponents δ and γ for the divergence of the time scales. The lower panel shows the exponents a and b for the master functions and the exponent parameter λ.

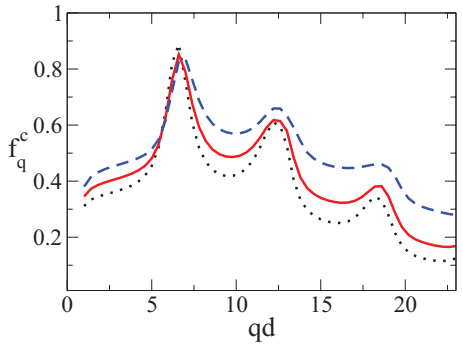

FIG. 8. (Color online) Critical glass-form factors f_q^c at the transition for $\varepsilon = 1.0$ (dotted curve), 0.5 (full curve), and 0.0 (dashed curve) in 2D.

V. TAGGED PARTICLE DYNAMICS

The results of granular MCT for the tagged particle dynamics has been discussed in II. Here, we will focus on the derivation of the MCT equations.

The incoherent scattering function $\phi_s(q,t)$ captures the tagged particle dynamics. This includes the mean-square displacement $\delta r^2(t) = \langle[\boldsymbol{r}_s - \boldsymbol{r}_s(t)]^2\rangle$ which appears as an expansion coefficient of the incoherent scattering function $\phi_s(q,t) = 1 - q^2\delta r^2(t)/6 + O(q^4)$ and the diffusivity $6D_\infty = \lim_{t\to\infty}\delta r^2(t)/t$ [52].

A. Equation of motion

Following the reasoning that one should account for the conserved quantities and only for the conserved quantities explicitly, one would assume that the equation of motion for a tagged particle should be first order in time. The density ρ_s is the only conserved quantity because the momentum of the tagged particle is all but conserved. It has been shown, though, that a consistent treatment of the tagged particle dynamics in fact requires an equation of motion which is second order in time [66,67], thus effectively reintroducing the tagged particle momentum as a macroscopic observable.

We follow that reasoning and introduce the incoherent projector

$$\mathcal{P}_s = \sum_{\boldsymbol{q}} |\rho_{\boldsymbol{q}}^s\rangle\langle\rho_{\boldsymbol{q}}^s| + \sum_{\boldsymbol{q}} |j_{\boldsymbol{q}}^{sL}\rangle\langle j_{\boldsymbol{q}}^{sL}|/T. \tag{40}$$

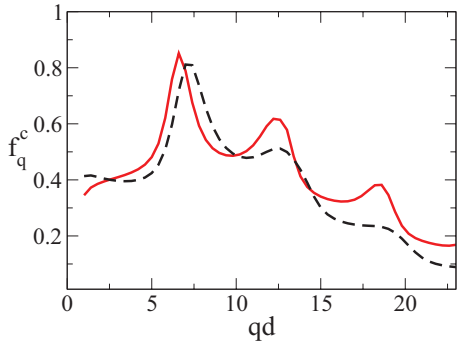

FIG. 9. (Color online) Critical glass-form factors f_q^c at the respective transition points for $\varepsilon = 0.5$ in 2D (full curve) and 3D (dashed curves).

Together with the microscopic state $\boldsymbol{a}_{\boldsymbol{q}}^s = (\rho_{\boldsymbol{q}}^s,\ j_{\boldsymbol{q}}^{sL}/\sqrt{T})$, it yields an equation of motion for $\phi_s(q,t)$ formally identical to Eq. (18):

$$\begin{aligned} 0 = {} & \ddot{\phi}_s(q,t) + \nu_q\dot{\phi}_s(q,t) + \Omega_s^s\phi_s(q,t) \\ & + \Omega_s^2\int_0^t d\tau\, m_s(q,t-\tau)\dot{\phi}_s(q,\tau) \\ & + \Omega_s^2\int_0^t d\tau\, L_s(q,t-\tau)\phi_s(q,\tau), \end{aligned} \tag{41}$$

with $\dot{\phi}_s(q,t=0) = 0$ and $\phi_s(q,t=0) = 1$. Moreover, $\Omega_{j\rho}^s = \langle j_{\boldsymbol{q}}^{sL}|\mathcal{L}_+\rho_{\boldsymbol{q}}^s\rangle/\sqrt{T} = q\sqrt{T}$ and $\Omega_{\rho j}^s = q\sqrt{T}$ do not depend on the coefficient of restitution, as shown in Appendix C 4. Hence, $\Omega_s^2 := \Omega_{j\rho}^s\Omega_{\rho j}^s = q^2T$ is identical to the corresponding quantity of the molecular fluid. This implies that looking at the probability density of the tagged particle on macroscopic time and length scales at very low densities, such that the memory kernel can be neglected, the microscopically broken time-reversal symmetry is unobservable.

The memory kernels are given by

$$m_s(q,t) = \langle F_{\boldsymbol{q}}^{s\dagger}|\tilde{\mathsf{U}}(t)F_{\boldsymbol{q}}^s\rangle/q^2T^2, \tag{42a}$$

$$L_s(q,t) = \langle J_{\boldsymbol{q}}^{s\dagger}|\tilde{\mathsf{U}}(t)F_{\boldsymbol{q}}^s\rangle/qT, \tag{42b}$$

with the fluctuating forces $F_{\boldsymbol{q}}^s = \mathcal{Q}_s\mathcal{L}_+j_{\boldsymbol{q}}^{sL}$ and $F_{\boldsymbol{q}}^{s\dagger} = \mathcal{Q}_s\mathcal{L}_+^\dagger j_{\boldsymbol{q}}^{sL}$ and the fluctuating current $J_{\boldsymbol{q}}^{s\dagger} = \mathcal{Q}_s\mathcal{L}_+^\dagger\rho_{\boldsymbol{q}}^s$.

B. Mode-coupling approximation

We introduce an approximate projection operator to describe the coupling between the tagged particle and the host fluid:

$$\mathcal{P}_2^s = \sum_{\boldsymbol{k}<\boldsymbol{p}} |\rho_{\boldsymbol{k}}\rho_{\boldsymbol{p}}^s\rangle\langle\rho_{\boldsymbol{k}}\rho_{\boldsymbol{p}}^s|/\langle\rho_{\boldsymbol{k}}\rho_{\boldsymbol{p}}^s|\rho_{\boldsymbol{k}}\rho_{\boldsymbol{p}}^s\rangle. \tag{43}$$

The corresponding mode-coupling approximation reads

$$\begin{aligned} \tilde{\mathsf{U}}(t) &\approx \mathcal{P}_2^s\tilde{\mathsf{U}}(t)\mathcal{P}_2^s \\ &\approx N\sum_{\boldsymbol{k},\boldsymbol{p}} |\rho_{\boldsymbol{k}}\rho_{\boldsymbol{p}}^s\rangle\phi(k,t)\phi_s(p,t)\langle\rho_{\boldsymbol{k}}\rho_{\boldsymbol{p}}^s|/S_k. \end{aligned} \tag{44}$$

Within the MCA we find that $L_s(q,t) = 0$ and

$$m_s[\phi,\phi_s](q,t) \approx \frac{1}{q^2T^2}\sum_{\boldsymbol{k},\boldsymbol{p}}\mathcal{V}_{\boldsymbol{qkp}}^s\mathcal{W}_{\boldsymbol{qkp}}^s\phi(k,t)\phi_s(p,t), \tag{45}$$

where

$$\mathcal{V}_{\boldsymbol{qkp}}^s = \sqrt{N/S_k}\langle j_{\boldsymbol{q}}^{sL}|\mathcal{L}_+\mathcal{Q}_s\rho_{\boldsymbol{k}}\rho_{\boldsymbol{p}}^s\rangle, \tag{46a}$$

$$\mathcal{W}_{\boldsymbol{qkp}}^s = \sqrt{N/S_k}\langle\rho_{\boldsymbol{k}}\rho_{\boldsymbol{p}}^s|\mathcal{Q}_s\mathcal{L}_+j_{\boldsymbol{q}}^{sL}\rangle. \tag{46b}$$

Here,

$$\mathcal{V}_{\boldsymbol{qkp}}^s = \frac{T}{\sqrt{NS_k}}(\hat{\boldsymbol{q}}\cdot\boldsymbol{k})(S_k - 1)\delta_{\boldsymbol{q},\boldsymbol{k}+\boldsymbol{p}}, \tag{47a}$$

is known from the literature [68–70] and one finds (cf. Appendix C 6)

$$\mathcal{W}_{\boldsymbol{qkp}}^s = \frac{1+\varepsilon}{2}\frac{T}{\sqrt{NS_k}}(\hat{\boldsymbol{q}}\cdot\boldsymbol{k})(S_k - 1)\delta_{\boldsymbol{q},\boldsymbol{k}+\boldsymbol{p}}. \tag{47b}$$

For the vertices, the loss of detailed balance reappears also for the tagged particle dynamics.

Together, Eqs. (47a) and (47b) yield

$$m_s[\phi,\phi_s](q,t) \approx \frac{1+\varepsilon}{2}\frac{n}{q^2}\int\frac{d^Dk}{(2\pi)^D} \times S_k(\hat{\boldsymbol{q}}\cdot\boldsymbol{k})^2 c_k^2\phi(k,t)\phi_s(|\boldsymbol{q}-\boldsymbol{k}|,t). \quad (48)$$

C. Approximate equation of motion

Finally, the equation of motion for the incoherent scattering function reads

$$\ddot{\phi}_s(q,t)+\nu_q\dot{\phi}_s(q,t)+\Omega_s^2\phi_s(q,t) + \Omega_s^2\int_0^\infty d\tau m_s[\phi,\phi_s](q,t-\tau)\dot{\phi}_s(q,\tau)=0, \quad (49)$$

capturing the coupling of the tagged particle dynamics to the dynamics of the host fluid as reported in II.

The tagged particle is enslaved to the host fluid on macroscopic time scales. Consequently, it also develops persistent correlations, $f_q^s=\lim_{t\to\infty}\phi_s(q,t)$, at the critical density φ_c. They can be calculated from the equation

$$\frac{f_q^s}{1-f_q^s}=m[f,f^s](q). \quad (50)$$

A detailed discussion of the solutions of Eqs. (49) and (50) was given in II.

VI. DISCUSSION

The granular MCT, which includes and extends MCT for elastic hard spheres, shows that the dynamics of a driven granular fluid is for one remarkably similar to the equilibrium dynamics and at the same time fundamentally different. It is similar in that there is always a glass transition, accompanied by the two-step relaxation scenario of dynamic correlation functions and diverging time scales. Because both the order parameter $f_q(\varepsilon)$ and especially the critical exponents $a(\varepsilon)$ and $b(\varepsilon)$ depend on the coefficient of restitution ε, already slightly dissipative interactions ($\varepsilon\lesssim 1$) destroy the universality of the dynamics on long time scales, which is observed in elastic systems with either Newtonian or Brownian dynamics [I, [71,72]]. The change of ε will be detectable even on macroscopic time scales, in particular by observing the exponent $b(\varepsilon)$. This shows that the combination of dissipative collisions and driving cannot be mapped to an effective elastic hard sphere system with an effective temperature T_{eff} conceivably different from the granular temperature T. Such a mapping would allow us to find a scaling function such that $\phi(q,t;\varepsilon)=\tilde{\phi}(q,t/t_0(\varepsilon))$.

The phase diagram in the (T,φ) plane is still an open problem. The jamming density is defined for athermal ($T=0$) systems, while the granular glass transition is independent of temperature but assumes a finite temperature $T>0$ to sustain a fluid phase. It is not obvious if and how they are connected. Our results suggest that the glass transition density φ_c is always strictly smaller than the quasistatic jamming density φ_J. However, MCT is known to underestimate φ_c. What happens for densities $\varphi\geqslant\varphi_c(\varepsilon)$ larger than the critical density? At the glass transition, the α-relaxation rate τ^{-1} diverges. Consequently, in every compression protocol using a small but finite compression rate, at some density the compression rate will be larger than the α-relaxation rate τ^{-1}. From then on, the evolution of the system will be restricted to a subset of phase space. The packings, which are reached from that subset by further compression will also be restricted to a subset of all packings and that might not even include those of highest density. Even if the ideal glass transition is destroyed by processes which are ignored within MCT, the enormous increase of relaxation times will be prohibitive for all practical purposes.

Apart from the Enskog term, Eqs. (21a) and (21b), the equations of motion are formally identical in two and three space dimensions. Hence the glass transition is qualitatively similar in two and three dimensions, with however different values for the critical density and the critical exponents. Compared to $D=3$, the glass-form factors f_q decay slower in reciprocal space for $D=2$, indicating a stronger localization in two space dimensions.

In the final equations of motion, Eqs. (34) and (49), the driving force appears only implicitly. While driving is crucial to achieve a stationary state, beyond that it does not alter the relaxation rates Ω_{ab}, Ω_{ab}^s and does not enter into the couplings to densities. Driving contributions would appear in the linear theory, if the (kinetic) energy, i.e., the granular temperature, was included as a dynamic field. However, this is hard to justify in a granular fluid, where kinetic energy is dissipated locally and hence not a hydrodynamic variable. In terms of the MCT, a coupling to the currents in $\mathcal{P}_2$ [Eq. (25)] would include explicit driving terms. Such a coupling was considered in the original mode-coupling approaches [73,74], but its relevance even in equilibrium fluids remains unclear.

VII. CONCLUSION AND OUTLOOK

We considered randomly driven inelastic smooth hard disks (in $D=2$) and spheres (in $D=3$). We systematically derived equations of motion for the coherent scattering function $\phi(q,t)$ and the incoherent scattering function $\phi_s(q,t)$.

The equations of motion are formally identical to the ones for elastic hard-sphere or disk fluids in thermal equilibrium but acquire a nontrivial dependence on the coefficient of restitution, ε. A transition to a glassy state, indicated by a nonzero value of the order parameter f_q appears through the bifurcation scenario of mode-coupling theory. Like in thermal equilibrium, the spatial dimension of the system only enters via the static structure factors. In both dimensions, the critical packing fraction increases the more dissipative the particles are.

The dynamics around the plateau in the scattering functions is described by power laws with exponents, which are functions of the coefficient of restitution, ε. Together with the ε dependence of the order parameter f_q, this shows that the dynamics fundamentally changes upon varying the coefficient of restitution. In contrast, the difference between Newtonian and Brownian dynamics in thermal equilibrium can be absorbed in the redefinition of the microscopic time scale. Also, a reduced long-wavelength speed of sound is predicted for granular fluids.

One can hardly expect to observe a glass transition in a fluid of monodisperse hard spheres because the system would quickly crystallize. To slow down crystal nucleation, usually binary mixtures with a small size difference are

used [75]. For fluids in thermal equilibrium, it was found that a MCT for mixtures does not yield results that differ drastically from those for the monodisperse idealization [76]. For mixtures of granular particles, a new complication will be the nonequipartition of energy between the mixture species [77,78].

So far we only derived equations for the correlation functions of spontaneous fluctuations. In a fluid in thermal equilibrium, this immediately entails knowledge about the corresponding response functions via the fluctuation dissipation theorem (FDT) [79]. In fact, a lot of the experimental measurements are concerned with response spectra [80]. The existence and form of a generalized FDT in driven granular fluids and more generally in systems far from equilibrium is a subject of active research [81].

It would certainly be desirable to weaken the assumptions made on the stationary phase space distribution function $\varrho(\Gamma)$. So far, we ignore correlations between the velocities of different particles which are known to be present in driven granular fluids [82]. In light of the fact that the single-particle velocity distribution function is well represented by a simple Gaussian, these correlations can presumably be neglected as a first approximation. More serious are the static correlations, such as $S(q)$, which are known from simulations to differ from their elastic counterparts used here. However, we can easily incorporate data for the simulated structure factors into our approach; work along these lines is in progress.

The results presented above deal with a specific, highly idealized system. It is a natural question to ask how robust these results are qualitatively. No qualitative changes are expected for a speed-dependent coefficient of restitution $\varepsilon = \varepsilon(v)$. Also, models that can be described by an effective coefficient of restitution [83] like, e.g., the spring-dashpot model are expected to show a nonequilibrium glass transition. The inclusion of interparticle friction or the treatment of different driving forces will likely pose a number of challenges. Such changes might lead to equations of motion and results qualitatively different from the ones discussed here.

ACKNOWLEDGMENTS

We thank an anonymous referee for pointing us to a potentially serious flaw in our approach and Reiner Kree for helping us to resolve it. We thank Jörg Bartnick for checking many of our calculations. We acknowledge financial support by the DFG (FG1394).

APPENDIX A: DOUBLE AVERAGE

The starting point is the coarse grained densities, $\overline{\rho}_{\boldsymbol{q}}(t)$, $\overline{\rho}^s_{\boldsymbol{q}}(t)$ which are defined as averages of Eqs. (4a) and (5a) over a microscopic time window. Then the dynamic scattering functions are introduced as expectation values with respect to the phase space distribution function

$$\tilde{\phi}(q,t',t) := N\langle\overline{\rho}_{-\boldsymbol{q}}(t')\overline{\rho}_{\boldsymbol{q}}(t)\rangle/\tilde{S}_q(t), \tag{A1a}$$

where $\tilde{S}_q(t) := N\langle\overline{\rho}_{-\boldsymbol{q}}(t)\overline{\rho}_{\boldsymbol{q}}(t)\rangle$ is the static structure factor, and

$$\tilde{\phi}_s(q,t',t) := \left\langle\overline{\rho}^s_{-\boldsymbol{q}}(t')\overline{\rho}^s_{\boldsymbol{q}}(t)\right\rangle. \tag{A1b}$$

Formally, the scattering functions depend on the trajectory of the random driving force up to time t, Ξ_t. This breaks the time-translation invariance of the correlation functions.

Following Ref. [84], we assume that the time average implicit in the coarse grained densities can be replaced by an ensemble average over all trajectories of the driving force Ξ_t:

$$\tilde{\phi}(q,\tau,\tau+t) \simeq \phi(q,t) := \langle\langle\rho_{-\boldsymbol{q}}(0)\rho_{\boldsymbol{q}}(t)\rangle_\Xi\rangle/S_q, \tag{A2a}$$

$$\tilde{\phi}_s(q,\tau,\tau+t) \simeq \phi_s(q,t) := \left\langle\left\langle\rho^s_{-\boldsymbol{q}}(0)\rho^s_{\boldsymbol{q}}(t)\right\rangle_\Xi\right\rangle, \tag{A2b}$$

and $S_q := \langle\langle\rho_{-\boldsymbol{q}}(\tau)\rho_{\boldsymbol{q}}(\tau)\rangle_\Xi\rangle$, independent of the time τ. With this definition, the scattering functions are time-translation invariant.

APPENDIX B: GRANULAR YVON-BORN-GREEN RELATION

The Yvon-Born-Green (YBG) relation between the pair and the triplet correlation functions follows from the identity

$$\nabla_1 g(r_{12}) = (\varrho^{-1}\nabla_{12}\varrho)g(r_{12}) + n\int d^D r_3\, g_3(\boldsymbol{r}_1,\boldsymbol{r}_2,\boldsymbol{r}_3)(\varrho^{-1}\nabla_{13}\varrho), \tag{B1}$$

where ϱ^{-1} is the pseudo-inverse of the distribution function [85]. For elastic hard spheres, where $\varrho(\Gamma) \propto \prod_{i<j}\Theta(r_{ij}-d)$ This yields the known relation [50]

$$\nabla_1 g(r_{12}) = \hat{\boldsymbol{r}}_{12}\delta(r_{12}-d)g(r_{12}) + n\int d^D r_3\,\hat{\boldsymbol{r}}_{13}\delta(r_{13}-d)g_3(\boldsymbol{r}_1,\boldsymbol{r}_2,\boldsymbol{r}_3). \tag{B2}$$

For the inelastic hard spheres, there must be an additional spatial dependence of the distribution function, depending on the coefficient of restitution, ε, or otherwise, e.g., the structure factor S_q would not depend on ε.

Overlapping configurations still have zero probability and, because of homogeneity, only relative distances play a role. Therefore, the distribution function will be of the form $\varrho(\Gamma) \propto \prod_{i<j}\Theta(r_{ij}-d)\vartheta_\varepsilon(r_{ij})$ with a unknown function $\vartheta_\varepsilon(r) > 0$. With this, we get a granular hard-sphere YBG relation:

$$\nabla_1 g(r_{12}) = \hat{\boldsymbol{r}}_{12}\delta(r_{12}-d)g(r_{12}) + g(r_{12})\nabla_1\ln\vartheta_\varepsilon(r_{12}) + n\int d^D r_3\,\hat{\boldsymbol{r}}_{13}\delta(r_{13}-d)g_3(\boldsymbol{r}_1,\boldsymbol{r}_2,\boldsymbol{r}_3) + n\int d^D r_3\, g_3(\boldsymbol{r}_1,\boldsymbol{r}_2,\boldsymbol{r}_3)\nabla_1\ln\vartheta_\varepsilon(r_{13}).$$

Unfortunately, virtually nothing is known about the function $\vartheta_\varepsilon(r)$. Therefore we use the elastic hard sphere YBG relation which means we make the nontrivial approximation

$$g(r_{12})\nabla_1\ln\vartheta_\varepsilon(r_{12}) \approx -n\int d^D r_3 g_3(\boldsymbol{r}_1,\boldsymbol{r}_2,\boldsymbol{r}_3)\nabla_1\ln\vartheta_\varepsilon(r_{13}), \tag{B3}$$

which may be more general than setting $\vartheta_\varepsilon(r) \equiv 1$.

On the next level, we have

$$\begin{aligned}\nabla_1 g_3(123) = {} & [\hat{\boldsymbol{r}}_{12}\delta(r_{12}-d)+\hat{\boldsymbol{r}}_{13}\delta(r_{13}-d)]g_3(123)\\ & + g_3(123)\nabla_1[\ln\vartheta_\varepsilon(r_{12})+\ln\vartheta_\varepsilon(r_{13})]\\ & + n\int d^D r_4 \hat{\boldsymbol{r}}_{14}\delta(r_{14}-d)g_4(1234)\\ & + n\int d^D r_4 g_4(1234)\nabla_1\ln\vartheta_\varepsilon(r_{14}),\end{aligned}$$

using the abbreviation $i \equiv \boldsymbol{r}_i$. In Eq. (C21) below, we use the approximation

$$\begin{aligned}& g_3(123)\nabla_1[\ln\vartheta_\varepsilon(r_{12})+\ln\vartheta_\varepsilon(r_{13})]\\ & \quad\approx -n\int d^D r_4 g_4(1234)\nabla_1\ln\vartheta_\varepsilon(r_{14}).\end{aligned}\tag{B4}$$

APPENDIX C: MATRIX ELEMENTS

1. Frequency Ω_{jj} in two dimensions

We have to determine

$$\left\langle j_{\boldsymbol{q}}^L\middle|\mathcal{L}_+ j_{\boldsymbol{q}}^L\right\rangle = i\frac{N(N-1)}{2}\left\langle j_{\boldsymbol{q}}^L\middle|\mathcal{T}_{12}^+ j_{\boldsymbol{q}}^L\right\rangle,\tag{C1}$$

where all other contributions vanish due to parity. Explicitly, this reads

$$\begin{aligned}\left\langle j_{\boldsymbol{q}}^L\middle|\mathcal{L}_+ j_{\boldsymbol{q}}^L\right\rangle = {} & \frac{1+\varepsilon}{2} i\,\langle(\hat{\boldsymbol{q}}\cdot\boldsymbol{v}_1)(\hat{\boldsymbol{q}}\cdot\hat{\boldsymbol{r}}_{12})(\hat{\boldsymbol{r}}_{12}\cdot\boldsymbol{v}_{12})^2\\ & \Theta(-\hat{\boldsymbol{r}}_{12}\cdot\boldsymbol{v}_{12})\delta(r_{12}-d)(e^{i\boldsymbol{q}\cdot\boldsymbol{r}_{12}}-1)\rangle,\end{aligned}\tag{C2}$$

where the three particle term vanishes, again, due to parity. Introducing the relative velocity $\boldsymbol{v} := (\boldsymbol{v}_1-\boldsymbol{v}_2)/\sqrt{2}$, the velocity averages can be evaluated

$$\begin{aligned}& \langle(\hat{\boldsymbol{q}}\cdot\boldsymbol{v}_1)(\hat{\boldsymbol{r}}_{12}\cdot\boldsymbol{v}_{12})^2\Theta(-\hat{\boldsymbol{r}}_{12}\cdot\boldsymbol{v}_{12})\rangle\\ & \quad = \sqrt{2}(\hat{\boldsymbol{q}}\cdot\hat{\boldsymbol{r}}_{12})\langle(\hat{\boldsymbol{r}}_{12}\cdot\boldsymbol{v}_{12})^3\,\Theta(-\hat{\boldsymbol{r}}_{12}\cdot\boldsymbol{v}_{12})\rangle\\ & \quad = \frac{\sqrt{2}}{2\pi T}(\hat{\boldsymbol{q}}\cdot\hat{\boldsymbol{r}}_{12})\int_0^\infty dv\int_{\pi/2}^{3\pi/2} d\varphi\, v^4\cos^3\varphi e^{-v^2/(2T)}\\ & \quad = -2T\sqrt{T/\pi}(\hat{\boldsymbol{q}}\cdot\hat{\boldsymbol{r}}_{12}).\end{aligned}\tag{C3}$$

The remaining spatial average reads

$$\begin{aligned}& \langle(\hat{\boldsymbol{q}}\cdot\hat{\boldsymbol{r}}_{12})^2\delta(r_{12}-d)(e^{i\boldsymbol{q}\cdot\boldsymbol{r}_{12}}-1)\rangle\\ & \quad = -\frac{d\chi}{V}\int_0^{2\pi} d\varphi\cos^2\varphi(1-e^{iqd\cos\varphi}).\end{aligned}\tag{C4}$$

One finds

$$\frac{1}{\pi}\int_0^{2\pi} d\varphi\cos^2\varphi e^{iz\cos\varphi} = -2\frac{d^2 J_0(z)}{dz^2},\tag{C5}$$

i.e.,

$$\langle(\hat{\boldsymbol{q}}\cdot\hat{\boldsymbol{r}}_{12})^2\delta(r_{12}-d)(e^{i\boldsymbol{q}\cdot\boldsymbol{r}_{12}}-1)\rangle = -\frac{\pi n d\chi}{N}[1+2J_0''(qd)].\tag{C6}$$

Collecting terms, one arrives at Eq. (21a).

2. Frequency $\Omega_{\rho j}$

The driving contribution vanishes and the free streaming contribution yields

$$\left\langle\rho_{\boldsymbol{q}}\middle|\mathcal{L}_0 j_{\boldsymbol{q}}^L\right\rangle = \frac{q}{N^2}\left\langle\sum_{j,k}(\hat{\boldsymbol{q}}\cdot\boldsymbol{v}_k)^2 e^{-i\boldsymbol{q}\cdot\boldsymbol{r}_{jk}}\right\rangle = qTS_q/N.\tag{C7}$$

The collisional contribution reads

$$\begin{aligned}& \frac{N(N-1)}{2}\left\langle\rho_{\boldsymbol{q}}\middle|\mathcal{T}_{12} j_{\boldsymbol{q}}^L\right\rangle\\ & \quad = \frac{1+\varepsilon}{4}\hat{\boldsymbol{q}}\cdot\left\langle(\hat{\boldsymbol{r}}_{12}\cdot\boldsymbol{v}_{12})^2\hat{\boldsymbol{r}}_{12}\,\Theta(-\hat{\boldsymbol{r}}_{12}\cdot\boldsymbol{v}_{12})\right.\\ & \qquad \left.\times\,\delta(r_{12}-d)\left(e^{i\boldsymbol{q}\cdot\boldsymbol{r}_2}-e^{i\boldsymbol{q}\cdot\boldsymbol{r}_1}\right)\sum_j e^{-i\boldsymbol{q}\cdot\boldsymbol{r}_j}\right\rangle.\end{aligned}\tag{C8}$$

The velocity integration yields a factor $T/2$ while the spatial average can be rewritten as

$$\begin{aligned}& \left\langle\hat{\boldsymbol{r}}_{12}\delta(r_{12}-d)(e^{i\boldsymbol{q}\cdot\boldsymbol{r}_2}-e^{i\boldsymbol{q}\cdot\boldsymbol{r}_1})\sum_j e^{-i\boldsymbol{q}\cdot\boldsymbol{r}_j}\right\rangle\\ & \quad = 2\langle\hat{\boldsymbol{r}}_{12}\delta(r_{12}-d)e^{-i\boldsymbol{q}\cdot\boldsymbol{r}_{12}}\rangle\\ & \qquad + 2(N-2)\langle\hat{\boldsymbol{r}}_{12}\delta(r_{12}-d)e^{-i\boldsymbol{q}\cdot\boldsymbol{r}_3}e^{i\boldsymbol{q}\cdot\boldsymbol{r}_2}\rangle.\end{aligned}\tag{C9}$$

Application of the YBG relation to the second term yields

$$\begin{aligned}& N\langle\hat{\boldsymbol{r}}_{12}\delta(r_{12}-d)e^{-i\boldsymbol{q}\cdot\boldsymbol{r}_3}e^{i\boldsymbol{q}\cdot\boldsymbol{r}_2}\rangle\\ & \quad = -\frac{1}{N}(S_q-1) - \langle\hat{\boldsymbol{r}}_{12}\delta(r_{12}-d)e^{-i\boldsymbol{q}\cdot\boldsymbol{r}_{12}}\rangle,\end{aligned}\tag{C10}$$

i.e., the second term in Eq. (C10) cancels the first term in Eq. (C9). Combining the remaining terms we arrive at Eq. (22b).

3. Vertex $\mathcal{W}_{qkp}$

Because the vertex is linear in $\boldsymbol{v}_i$, there is no contribution from the driving $i\mathcal{L}_D^+$. Expanding the projector $\mathcal{Q}_c$, the vertex reads

$$\begin{aligned}\mathcal{W}_{\boldsymbol{qkp}} = {} & N\left\langle\rho_{\boldsymbol{k}}\rho_{\boldsymbol{p}}\middle|\mathcal{L}_+ j_{\boldsymbol{q}}^L\right\rangle/S_p\\ & - N^2\langle\rho_{\boldsymbol{k}}\rho_{\boldsymbol{p}}|\rho_{\boldsymbol{q}}\rangle\left\langle\rho_{\boldsymbol{q}}\middle|\mathcal{L}_+ j_{\boldsymbol{q}}^L\right\rangle/S_pS_q.\end{aligned}\tag{C11}$$

The free streaming contribution to the first term is given by

$$\begin{aligned}\left\langle\rho_{\boldsymbol{k}}\rho_{\boldsymbol{p}}\middle|\mathcal{L}_0 j_{\boldsymbol{q}}^L\right\rangle &= qT\langle\rho_{\boldsymbol{k}}\rho_{\boldsymbol{p}}|\rho_{\boldsymbol{q}}\rangle\\ &= \frac{qT}{N^2}\delta_{\boldsymbol{k}+\boldsymbol{p},\boldsymbol{q}}S^{(3)}(\boldsymbol{k},\boldsymbol{p}).\end{aligned}\tag{C12}$$

For the collisional contribution we find

$$\begin{aligned}& \frac{N(N-1)}{2}\left\langle\rho_{\boldsymbol{k}}\rho_{\boldsymbol{p}}\middle|\mathcal{T}_{12}^+ j_{\boldsymbol{q}}^L\right\rangle\\ & \quad = i\frac{1+\varepsilon}{4N}T\hat{\boldsymbol{q}}\cdot\left\langle\sum_{j,k}e^{-i\boldsymbol{k}\cdot\boldsymbol{r}_j}e^{-i\boldsymbol{p}\cdot\boldsymbol{r}_k}\hat{\boldsymbol{r}}_{12}\right.\\ & \qquad \left.\times\,\delta(r_{12}-d)(e^{i\boldsymbol{q}\cdot\boldsymbol{r}_2}-e^{i\boldsymbol{q}\cdot\boldsymbol{r}_1})\right\rangle.\end{aligned}\tag{C13}$$

The average on the right-hand side shall be abbreviated as $\langle jk|12\rangle$. Then this can be expanded as

$$\begin{aligned}\langle jk|12\rangle = {} & \langle 11|12\rangle + \langle 22|12\rangle + \langle 12|12\rangle + \langle 21|12\rangle \\ & + N(\langle 13|12\rangle + \langle 23|12\rangle + \langle 31|12\rangle + \langle 32|12\rangle) \\ & + N\langle 33|12\rangle + N^2\langle 34|12\rangle. \end{aligned} \tag{C14}$$

Exploiting the symmetries, this can be simplified to

$$\begin{aligned}\langle jk|12\rangle = {} & 2\langle 11|12\rangle + \langle 12|12\rangle + 2N\langle 13|12\rangle \\ & + N\langle 33|12\rangle + N^2\langle 34|12\rangle. \end{aligned} \tag{C15}$$

Proceeding term by term we first find

$$\langle 11|12\rangle = \langle e^{i(\boldsymbol{k}+\boldsymbol{p}-\boldsymbol{q})\cdot\boldsymbol{r}_1}\hat{\boldsymbol{r}}_{12}\delta(r_{12}-d)(e^{i\boldsymbol{q}\cdot\boldsymbol{r}_{12}}-1)\rangle,$$

which can be reduced to

$$\begin{aligned}\langle 11|12\rangle &= \delta_{\boldsymbol{k}+\boldsymbol{p},\boldsymbol{q}}\langle\hat{\boldsymbol{r}}_{12}\delta(r_{12}-d)e^{i\boldsymbol{q}\cdot\boldsymbol{r}_{12}}\rangle \\ &\equiv \delta_{\boldsymbol{k}+\boldsymbol{p},\boldsymbol{q}}\boldsymbol{G}(\boldsymbol{q}). \end{aligned} \tag{C16}$$

The second term can be reduced to an equivalent expression

$$\begin{aligned}\langle 12|12\rangle = {} & \langle e^{i(\boldsymbol{k}+\boldsymbol{p}-\boldsymbol{q})\cdot\boldsymbol{r}_1}\hat{\boldsymbol{r}}_{12}\delta(r_{12}-d)e^{i\boldsymbol{q}\cdot\boldsymbol{r}_{12}}\rangle \\ & - \langle e^{i(\boldsymbol{k}+\boldsymbol{p}-\boldsymbol{q})\cdot\boldsymbol{r}_1}\hat{\boldsymbol{r}}_{12}\delta(r_{12}-d)e^{i(\boldsymbol{k}-\boldsymbol{q})\cdot\boldsymbol{r}_{12}}\rangle, \end{aligned}$$

i.e.,

$$\langle 12|12\rangle = \delta_{\boldsymbol{k}+\boldsymbol{p},\boldsymbol{q}}[\boldsymbol{G}(\boldsymbol{k})+\boldsymbol{G}(\boldsymbol{p})]. \tag{C17}$$

The first three-particle term

$$\begin{aligned}\langle 13|12\rangle = {} & \langle e^{i(\boldsymbol{k}+\boldsymbol{p}-\boldsymbol{q})\cdot\boldsymbol{r}_2}e^{i\boldsymbol{k}\cdot\boldsymbol{r}_{12}}e^{i\boldsymbol{p}\cdot\boldsymbol{r}_{32}}\hat{\boldsymbol{r}}_{12}\delta(r_{12}-d)\rangle \\ & - \langle e^{i(\boldsymbol{k}-\boldsymbol{q})\cdot\boldsymbol{r}_1}e^{i\boldsymbol{p}\cdot\boldsymbol{r}_3}\hat{\boldsymbol{r}}_{12}\delta(r_{12}-d)\rangle \end{aligned}$$

requires a little more work. The first term shall be abbreviated as

$$\langle e^{i(\boldsymbol{k}+\boldsymbol{p}-\boldsymbol{q})\cdot\boldsymbol{r}_2}e^{i\boldsymbol{k}\cdot\boldsymbol{r}_{12}}e^{i\boldsymbol{p}\cdot\boldsymbol{r}_{32}}\hat{\boldsymbol{r}}_{12}\delta(r_{12}-d)\rangle = \delta_{\boldsymbol{k}+\boldsymbol{p},\boldsymbol{q}}\boldsymbol{H}(\boldsymbol{k},\boldsymbol{p}). \tag{C18}$$

The second term can be simplified with the help of the YBG relation:

$$\begin{aligned}&\langle e^{i(\boldsymbol{k}-\boldsymbol{q})\cdot\boldsymbol{r}_1}e^{i\boldsymbol{p}\cdot\boldsymbol{r}_3}\hat{\boldsymbol{r}}_{12}\delta(r_{12}-d)\rangle \\ &\quad = \frac{1}{N^2}\delta_{\boldsymbol{k}+\boldsymbol{p},\boldsymbol{q}}[i\boldsymbol{p}(S_p-1)+N\boldsymbol{G}(\boldsymbol{p})]. \end{aligned} \tag{C19}$$

Similarly, the second three-particle term

$$\langle 33|12\rangle = \langle e^{i(\boldsymbol{k}+\boldsymbol{p})\cdot\boldsymbol{r}_3}\hat{\boldsymbol{r}}_{12}\delta(r_{12}-d)(e^{-i\boldsymbol{q}\cdot\boldsymbol{r}_2}-e^{-i\boldsymbol{q}\cdot\boldsymbol{r}_1})\rangle$$

can be reduced by employing the YBG relation

$$\langle 33|12\rangle = -\frac{2}{N^2}\delta_{\boldsymbol{k}+\boldsymbol{p},\boldsymbol{q}}[i\boldsymbol{q}(S_q-1)+N\boldsymbol{G}(\boldsymbol{q})]. \tag{C20}$$

The four-particle term

$$\langle 34|12\rangle = \langle e^{i\boldsymbol{k}\cdot\boldsymbol{r}_3}e^{i\boldsymbol{p}\cdot\boldsymbol{r}_4}\hat{\boldsymbol{r}}_{12}\delta(r_{12}-d)(e^{-i\boldsymbol{q}\cdot\boldsymbol{r}_2}-e^{-i\boldsymbol{q}\cdot\boldsymbol{r}_1})\rangle$$

is naturally the most involved. Using the higher-order YBG relation it reads

$$\begin{aligned}\langle 34|12\rangle = {} & -\frac{2}{NV^3}\int d^Dr_2d^Dr_3d^Dr_4e^{-i\boldsymbol{q}\cdot\boldsymbol{r}_2}e^{i\boldsymbol{k}\cdot\boldsymbol{r}_3}e^{i\boldsymbol{p}\cdot\boldsymbol{r}_4}\frac{\partial}{\partial\boldsymbol{r}_2}g_3(\boldsymbol{r}_2,\boldsymbol{r}_3,\boldsymbol{r}_4) \\ & + \frac{2}{NV^3}\int d^Dr_2d^Dr_3d^Dr_4e^{-i\boldsymbol{q}\cdot\boldsymbol{r}_2}e^{i\boldsymbol{k}\cdot\boldsymbol{r}_3}e^{i\boldsymbol{p}\cdot\boldsymbol{r}_4}\hat{\boldsymbol{r}}_{23}\delta(r_{23}-d)g_3(\boldsymbol{r}_2,\boldsymbol{r}_3,\boldsymbol{r}_4) \\ & + \frac{2}{NV^3}\int d^Dr_2d^Dr_3d^Dr_4e^{-i\boldsymbol{q}\cdot\boldsymbol{r}_2}e^{i\boldsymbol{k}\cdot\boldsymbol{r}_3}e^{i\boldsymbol{p}\cdot\boldsymbol{r}_4}\hat{\boldsymbol{r}}_{24}\delta(r_{24}-d)g_3(\boldsymbol{r}_2,\boldsymbol{r}_3,\boldsymbol{r}_4). \end{aligned} \tag{C21}$$

Partial integration in the first term and the extraction of the momentum conservation constraint yields

$$\begin{aligned}\langle 34|12\rangle = {} & -\frac{2i\boldsymbol{q}}{NV^2}\delta_{\boldsymbol{k}+\boldsymbol{p},\boldsymbol{q}}\int d^Dr_{23}d^Dr_{24}e^{-i\boldsymbol{k}\cdot\boldsymbol{r}_{23}}e^{-i\boldsymbol{p}\cdot\boldsymbol{r}_{24}}g_3(\boldsymbol{r}_{23},\boldsymbol{r}_{24}) \\ & + \frac{2}{NV^2}\delta_{\boldsymbol{k}+\boldsymbol{p},\boldsymbol{q}}\int d^Dr_{23}d^Dr_{24}e^{-i\boldsymbol{k}\cdot\boldsymbol{r}_{23}}e^{-i\boldsymbol{p}\cdot\boldsymbol{r}_{24}}g_3(\boldsymbol{r}_{23},\boldsymbol{r}_{24})\hat{\boldsymbol{r}}_{23}\delta(r_{23}-d) \\ & + \frac{2}{NV^2}\delta_{\boldsymbol{k}+\boldsymbol{p},\boldsymbol{q}}\int d^Dr_{23}d^Dr_{24}e^{-i\boldsymbol{k}\cdot\boldsymbol{r}_{23}}e^{-i\boldsymbol{p}\cdot\boldsymbol{r}_{24}}g_3(\boldsymbol{r}_{23},\boldsymbol{r}_{24})\hat{\boldsymbol{r}}_{24}\delta(r_{24}-d). \end{aligned} \tag{C22}$$

This leaves us with the relatively simple expression

$$\begin{aligned}\langle 34|12\rangle = {} & -\frac{2i\boldsymbol{q}}{N^3}\delta_{\boldsymbol{k}+\boldsymbol{p},\boldsymbol{q}}[S^{(3)}(\boldsymbol{k},\boldsymbol{p})-S_k-S_p-S_q+2] \\ & -\frac{2}{N}\delta_{\boldsymbol{k}+\boldsymbol{p},\boldsymbol{q}}[\boldsymbol{H}(\boldsymbol{k},\boldsymbol{p})+\boldsymbol{H}(\boldsymbol{p},\boldsymbol{k})]. \end{aligned}$$

Most terms cancel to yield

$$\langle jk|12\rangle = \frac{2i}{N}\delta_{\boldsymbol{k}+\boldsymbol{p},\boldsymbol{q}}[\boldsymbol{k}S_p+\boldsymbol{p}S_k-\boldsymbol{q}S^{(3)}(\boldsymbol{k},\boldsymbol{p})], \tag{C23}$$

or

$$\begin{aligned}&\frac{N(N-1)}{2}\langle\rho_k\rho_p|\mathcal{T}_{12}^+j_q^L\rangle \\ &\quad = -\frac{1+\varepsilon}{2}\frac{T}{N^2}[(\hat{\boldsymbol{q}}\cdot\boldsymbol{k})S_p+(\hat{\boldsymbol{q}}\cdot\boldsymbol{p})S_k-qS^{(3)}(\boldsymbol{k},\boldsymbol{p})]. \end{aligned} \tag{C24}$$

Inserting Eqs. (C12) and (C24) into Eq. (C11) and applying the convolution approximation yields Eq. (31b).

4. Frequency $\Omega^s_{\rho j}$

The free streaming contribution reads

$$\langle \rho^s_{\boldsymbol{q}} | \mathcal{L}_0 j^{sL}_{\boldsymbol{q}} \rangle = q \langle (\hat{\boldsymbol{q}} \cdot \boldsymbol{v}_s)^2 \rangle = qT, \tag{C25}$$

and the collisional contribution

$$(N-1)\langle \rho^s_{\boldsymbol{q}} \mathcal{T}^+_{1s} j^{sL}_{\boldsymbol{q}} \rangle = i \frac{1+\varepsilon}{2} N \langle (\hat{\boldsymbol{r}}_{1s} \cdot \boldsymbol{v}_{1s})^2 (\hat{\boldsymbol{q}} \cdot \hat{\boldsymbol{r}}_{1s}) \Theta(-\hat{\boldsymbol{r}}_{1s} \cdot \boldsymbol{v}_{1s}) \delta(r_{1s} - d) \rangle = 0 \tag{C26}$$

vanishes due to symmetry.

5. Vertex $\mathcal{V}^s_{\boldsymbol{q}\boldsymbol{k}\boldsymbol{p}}$

The left incoherent vertex is given as

$$\mathcal{V}^s_{\boldsymbol{q}\boldsymbol{k}\boldsymbol{p}} = \langle j^{sL}_{\boldsymbol{q}} | \mathcal{L}_+ \rho_{\boldsymbol{k}} \rho^s_{\boldsymbol{p}} \rangle - \langle j^{sL}_{\boldsymbol{q}} | \mathcal{L}_+ \rho^s_{\boldsymbol{q}} \rangle \langle \rho^s_{\boldsymbol{q}} | \rho_{\boldsymbol{k}} \rho^s_{\boldsymbol{p}} \rangle. \tag{C27}$$

The triple density correlator,

$$\langle \rho^s_{\boldsymbol{q}} | \rho_{\boldsymbol{k}} \rho^s_{\boldsymbol{p}} \rangle = \frac{1}{N} \delta_{\boldsymbol{k}+\boldsymbol{p},\boldsymbol{q}} S_k, \tag{C28}$$

is related to the structure factor. Moreover, we have

$$\langle j^{sL}_{\boldsymbol{q}} | \mathcal{L}_+ \rho_{\boldsymbol{k}} \rho^s_{\boldsymbol{p}} \rangle = k \langle j^{sL}_{\boldsymbol{q}} | j^L_{\boldsymbol{k}} \rho^s_{\boldsymbol{p}} \rangle + p \langle j^{sL}_{\boldsymbol{q}} | \rho_{\boldsymbol{k}} j^{sL}_{\boldsymbol{p}} \rangle \tag{C29}$$

as only the free streaming operator $i\mathcal{L}_0$ applies. The velocity integration yields a factor of T:

$$\begin{aligned} \langle j^{sL}_{\boldsymbol{q}} | \mathcal{L}_+ \rho_{\boldsymbol{k}} \rho^s_{\boldsymbol{p}} \rangle &= \frac{kT}{N} \langle \rho^s_{\boldsymbol{q}} | \rho^s_{\boldsymbol{k}} \rho^s_{\boldsymbol{p}} \rangle + pT \langle \rho^s_{\boldsymbol{q}} | \rho_{\boldsymbol{k}} \rho^s_{\boldsymbol{p}} \rangle \\ &= \frac{1}{N} [(\hat{\boldsymbol{q}} \cdot \boldsymbol{k}) T + (\hat{\boldsymbol{q}} \cdot \boldsymbol{p}) S_k] \delta_{\boldsymbol{k}+\boldsymbol{p},\boldsymbol{q}}. \end{aligned} \tag{C30}$$

Collecting terms one arrives at Eq. (47a).

6. Vertex $\mathcal{W}^s_{\boldsymbol{q}\boldsymbol{k}\boldsymbol{p}}$

The incoherent vertex is given as

$$\mathcal{W}^s_{\boldsymbol{q}\boldsymbol{k}\boldsymbol{p}} = \langle \rho_{\boldsymbol{k}} \rho^s_{\boldsymbol{p}} | \mathcal{L}_+ j^{sL}_{\boldsymbol{q}} \rangle - \langle \rho_{\boldsymbol{k}} \rho^s_{\boldsymbol{p}} | \rho^s_{\boldsymbol{q}} \rangle \langle \rho^s_{\boldsymbol{q}} | \mathcal{L}_+ j^{sL}_{\boldsymbol{q}} \rangle. \tag{C31}$$

The free streaming contribution is simple:

$$\langle \rho_{\boldsymbol{k}} \rho^s_{\boldsymbol{p}} | \mathcal{L}_0 j^{sL}_{\boldsymbol{q}} \rangle = qT \langle \rho_{\boldsymbol{k}} \rho^s_{\boldsymbol{p}} | \rho^s_{\boldsymbol{q}} \rangle = \frac{qT}{N} \delta_{\boldsymbol{k}+\boldsymbol{p},\boldsymbol{q}} S_k. \tag{C32}$$

For the collisional part one finds with the velocity integration being already performed:

$$\begin{aligned} &(N-1)\langle \rho_{\boldsymbol{k}} \rho^s_{\boldsymbol{p}} | \mathcal{T}^+_{1s} j^{sL}_{\boldsymbol{q}} \rangle \\ &= i \frac{1+\varepsilon}{2} \frac{T}{N} \left\langle \sum_j e^{-i\boldsymbol{k}\cdot\boldsymbol{r}_j} e^{-i(\boldsymbol{p}-\boldsymbol{q})\cdot\boldsymbol{r}_s} (\hat{\boldsymbol{q}} \cdot \boldsymbol{r}_{1s}) \delta(r_{1s} - d) \right\rangle \\ &= i \frac{1+\varepsilon}{2} \frac{T}{N} \delta_{\boldsymbol{k}+\boldsymbol{p}-\boldsymbol{q}} \left\langle \sum_j e^{-i\boldsymbol{k}\cdot\boldsymbol{r}_{js}} (\hat{\boldsymbol{q}} \cdot \boldsymbol{r}_{1s}) \delta(r_{1s} - d) \right\rangle. \end{aligned} \tag{C33}$$

The spatial average,

$$\begin{aligned} &\left\langle \sum_j e^{-i\boldsymbol{k}\cdot\boldsymbol{r}_{js}} (\hat{\boldsymbol{q}} \cdot \boldsymbol{r}_{1s}) \delta(r_{1s} - d) \right\rangle \\ &= \langle e^{-i\boldsymbol{k}\cdot\boldsymbol{r}_{1s}} (\hat{\boldsymbol{q}} \cdot \boldsymbol{r}_{1s}) \delta(r_{1s} - d) \rangle \\ &\quad + N \langle e^{-i\boldsymbol{k}\cdot\boldsymbol{r}_{2s}} (\hat{\boldsymbol{q}} \cdot \boldsymbol{r}_{1s}) \delta(r_{1s} - d) \rangle, \end{aligned} \tag{C34}$$

can again be evaluated with the help of the YBG relation. Applying it to the second term cancels the first term and we get

$$(N-1)\langle \rho_{\boldsymbol{k}} \rho^s_{\boldsymbol{p}} | \mathcal{T}^+_{1s} j^{sL}_{\boldsymbol{q}} \rangle = \frac{1+\varepsilon}{2} \frac{T}{N} \delta_{\boldsymbol{k}+\boldsymbol{p}-\boldsymbol{q}} (\hat{\boldsymbol{q}} \cdot \boldsymbol{k})(S_k - 1). \tag{C35}$$

Collecting terms one arrives at Eq. (47b).

APPENDIX D: DETAILS OF NUMERICS

For the numerical solution of Eqs. (34), (35), and (49), we used well-established algorithms in 3D [60] and 2D [65]. Reciprocal space is discretized into M^3 grid points ($M = 100$) up to a cutoff of $qd = 40$ in 3D, and with $M = 125$ up a cutoff of $qd = 50$ in 2D. The time axis is also discrete with a grid of $N = 2048$ points and a step size that is doubled in successive steps to accommodate for logarithmic time scales. The initial time step is $\Delta t = 10^{-9} t_0$. The critical density φ_c is located by interval bisection.

[1] A. L. Greer, Science **267**, 1947 (1995).
[2] W. van Megen, Transp. Theory Stat. Phys. **24**, 1017 (1995).
[3] R. Höhler and S. Cohen-Addad, J. Phys.: Condens. Matter **17**, R1041 (2005).
[4] G. Marty and O. Dauchot, Phys. Rev. Lett. **94**, 015701 (2005).
[5] A. R. Abate and D. J. Durian, Phys. Rev. E **74**, 031308 (2006).
[6] D. I. Goldman and H. L. Swinney, Phys. Rev. Lett. **96**, 145702 (2006).
[7] P. M. Reis, R. A. Ingale, and M. D. Shattuck, Phys. Rev. Lett. **98**, 188301 (2007).
[8] A. S. Keys, A. R. Abate, S. C. Glotzer, and D. J. Durian, Nat. Phys. **3**, 260 (2007).
[9] W. T. Kranz, M. Sperl, and A. Zippelius, Phys. Rev. Lett. **104**, 225701 (2010).
[10] M. Sperl, W. T. Kranz, and A. Zippelius, Europhys. Lett. **98**, 28001 (2012).
[11] P. N. Pusey and W. van Megen, Nature (London) **320**, 340 (1986).
[12] P. G. Debenedetti and F. H. Stillinger, Nature (London) **410**, 259 (2001).
[13] A. Cavagna, Phys. Rep. **476**, 51 (2009).
[14] W. Götze, *Complex Dynamics of Glass-Forming Liquids: A Mode-Coupling Theory* (Oxford University Press, Oxford, 2009).
[15] M. Fuchs and M. E. Cates, Phys. Rev. Lett. **89**, 248304 (2002).
[16] M. Fuchs and M. E. Cates, J. Rheol. (Melville, NY, US) **53**, 957 (2009).
[17] A. Habdas, D. Schaar, A. Levitt, and E. Weeks, Europhys. Lett. **67**, 477 (2004).
[18] I. Gazuz, A. M. Puertas, T. Voigtmann, and M. Fuchs, Phys. Rev. Lett. **102**, 248302 (2009).
[19] R. Candelier and O. Dauchot, Phys. Rev. Lett. **103**, 128001 (2009).

[20] M. E. Cates, J. P. Wittmer, J.-P. Bouchaud, and P. Claudin, Phys. Rev. Lett. **81**, 1841 (1998).

[21] M. Pica Ciamarra, M. Nicodemi, and A. Coniglio, Soft Matter **6**, 2871 (2010).

[22] A. J. Liu and S. R. Nagel, Nature (London) **396**, 21 (1998).

[23] C. S. O'Hern, L. E. Silbert, A. J. Liu, and S. R. Nagel, Phys. Rev. E **68**, 011306 (2003).

[24] R. M. Iverson, Rev. Geophys. **35**, 245 (1997).

[25] A. Prevost, D. A. Egolf, and J. S. Urbach, Phys. Rev. Lett. **89**, 084301 (2002).

[26] I. S. Aranson and J. S. Olafsen, Phys. Rev. E **66**, 061302 (2002).

[27] K. Kohlstedt, A. Snezhko, M. V. Sapozhnikov, I. S. Aranson, J. S. Olafsen, and E. Ben-Naim, Phys. Rev. Lett. **95**, 068001 (2005).

[28] C. C. Maaß, N. Isert, G. Maret, and C. M. Aegerter, Phys. Rev. Lett. **100**, 248001 (2008).

[29] R. P. Ojha, P. A. Lemieux, P. K. Dixon, A. J. Liu, and D. J. Durian, Nature (London) **427**, 521 (2004).

[30] A. R. Abate and D. J. Durian, Phys. Rev. E **72**, 031305 (2005).

[31] M. Schröter, D. I. Goldman, and H. L. Swinney, Phys. Rev. E **71**, 030301 (2005).

[32] P. K. Haff, J. Fluid Mech. **134**, 401 (1983).

[33] S. McNamara, Phys. Fluids A **5**, 3056 (1993).

[34] I. Goldhirsch and G. Zanetti, Phys. Rev. Lett. **70**, 1619 (1993).

[35] We use the convention $\mathsf{FT}[f](\boldsymbol{k}) = \int f(\boldsymbol{r}) e^{-i\boldsymbol{k}\cdot\boldsymbol{r}} d^D r$.

[36] A. R. Altenberger, Phys. A (Amsterdam, Neth.) **80**, 46 (1975).

[37] T. Aspelmeier, M. Huthmann, and A. Zippelius, in *Granular Gases*, edited by T. Pöschel and S. Luding (Springer, Berlin, 2001) pp. 31–58.

[38] M. H. Ernst, J. R. Dorfmann, W. R. Hoegy, and J. M. J. van Leeuwen, Physica **45**, 127 (1969).

[39] B. J. West, A. R. Bulsara, K. Lindenberg, V. Seshadri, and K. E. Shuler, Phys. A (Amsterdam, Neth.) **97**, 211 (1979).

[40] J. K. Percus and G. J. Yevick, Phys. Rev. **110**, 1 (1958).

[41] N. W. Ashcroft and J. Lekner, Phys. Rev. **145**, 83 (1966).

[42] N. F. Carnahan and K. E. Starling, J. Chem. Phys. **51**, 635 (1969).

[43] M. Baus and J. L. Colot, Phys. Rev. A **36**, 3912 (1987).

[44] We use the convention $\hat{f}(s) = \mathsf{LT}[f](s) = i\int_0^\infty f(t) e^{-ist} dt$.

[45] H. Mori, Prog. Theor. Phys. **34**, 399 (1965).

[46] S. Chapman and T. G. Cowling, *The Mathematical Theory of Non-Uniform Gases* (Cambridge University Press, Cambridge, 1960).

[47] E. Leutheusser, J. Phys. C: Solid State Phys. **15**, 2801 (1982) .

[48] *Gradshteyn and Ryzhik's Table of Integrals, Series, and Products*, edited by A. Jeffrey and D. Zwillinger, 6th ed. (Academic Press, San Diego, 2000).

[49] A factor of 2/3 was missing in I & II. This has no influence on the results discussed there.

[50] J.-P. Hansen and I. R. McDonald, *Theory of Simple Liquids*, 3rd ed. (Academic Press, Amsterdam, 2006).

[51] K. S. Schweizer and J. G. Curro, Phys. Rev. Lett. **60**, 809 (1988).

[52] J. P. Boon and S. Yip, *Molecular Hydrodynamics* (Dover Publications, New York, 1992).

[53] T. P. C. van Noije, M. H. Ernst, E. Trizac, and I. Pagonabarraga, Phys. Rev. E **59**, 4326 (1999).

[54] M. Fixman, J. Chem. Phys. **36**, 310 (1962).

[55] K. Kawasaki, Phys. Rev. **150**, 291 (1966).

[56] L. P. Kadanoff and J. Swift, Phys. Rev. **166**, 89 (1968).

[57] J. Bosse, W. Götze, and M. Lücke, Phys. Rev. A **17**, 434 (1978).

[58] J. L. Barrat, W. Götze, and A. Latz, J. Phys.: Condens. Matter **1**, 7163 (1989).

[59] H. W. Jackson and E. Feenberg, Rev. Mod. Phys. **34**, 686 (1962).

[60] T. Franosch, M. Fuchs, W. Götze, M. R. Mayr, and A. P. Singh, Phys. Rev. E **55**, 7153 (1997).

[61] W. Götze and L. Sjögren, J. Math. Anal. Appl. **195**, 230 (1995).

[62] G. Williams and D. C. Watts, Trans. Faraday Soc. **66**, 80 (1970).

[63] M. Fuchs, J. Non-Cryst. Solids **172**, 241 (1994).

[64] M. Sperl, Phys. Rev. E **68**, 031405 (2003).

[65] M. Bayer, J. M. Brader, F. Ebert, M. Fuchs, E. Lange, G. Maret, R. Schilling, M. Sperl, and J. P. Wittmer, Phys. Rev. E **76**, 011508 (2007).

[66] B. Cichocki and W. Hess, Phys. A (Amsterdam, Neth.) **141**, 475 (1987).

[67] S. J. Pitts and H. C. Andersen, J. Chem. Phys. **113**, 3945 (2000).

[68] G. Wahnström and L. Sjögren, J. Phys. C **15**, 401 (1982).

[69] U. Bengtzelius, W. Götze, and A. Sjölander, J. Phys. C: Solid State Phys. **17**, 5915 (1984).

[70] We are not aware of a published derivation within the projection operator formalism, though. We present it in appendix C 5.

[71] H. Löwen, J. P. Hansen, and J. N. Roux, Phys. Rev. A **44**, 1169 (1991).

[72] T. Gleim, W. Kob, and K. Binder, Phys. Rev. Lett. **81**, 4404 (1998).

[73] G. F. Mazenko, Phys. Rev. A **9**, 360 (1974).

[74] L. Sjögren, Phys. Rev. A **22**, 2866 (1980).

[75] E. Zaccarelli, C. Valeriani, E. Sanz, W. C. K. Poon, M. E. Cates, and P. N. Pusey, Phys. Rev. Lett. **103**, 135704 (2009).

[76] J. L. Barrat and A. Latz, J. Phys.: Condens. Matter **2**, 4289 (1990).

[77] A. Barrat and E. Trizac, Granular Matter **4**, 57 (2002).

[78] H. Uecker, W. T. Kranz, T. Aspelmeier, and A. Zippelius, Phys. Rev. E **80**, 041303 (2009).

[79] S. R. de Groot and P. Mazur, *Non-Equilibrium Thermodynamics* (Dover Publications, Inc., New York, 1984).

[80] J. Jäckle, Rep. Prog. Phys. **49**, 171 (1986).

[81] U. M. B. Marconi, A. Puglisi, L. Rondoni, and A. Vulpiani, Phys. Rep. **461**, 111 (2008).

[82] I. Pagonabarraga, E. Trizac, T. P. C. van Noije, and M. H. Ernst, Phys. Rev. E **65**, 011303 (2001).

[83] J. Schäfer, S. Dippel, and D. E. Wolf, J. Phys. I **6**, 5 (1996).

[84] A. J. Archer and M. Rauscher, J. Phys. A **37**, 9325 (2004).

[85] M. Born and H. S. Green, Proc. R. Soc. London, Ser. A **188**, 10 (1946).